Modeling of Recovery and In-situ Distribution of Fracturing Fluid in Shale Gas Reservoirs Due to Fracture Closure, Proppant Distribution and Gravity Segregation

by

Yongzan Liu

A thesis submitted in partial fulfillment of the requirements for the degree of

Master of Science

in

Petroleum Engineering

Department of Civil and Environmental Engineering
University of Alberta

Abstract

Many stimulated shale gas wells experience surprisingly low fracturing fluid recoveries. Fracture closure, gravity segregation, fracture tortuosity, proppant distribution, drawdown pressure and shut-in (soaking) duration have been widely postulated to be the contributing factors. Despite propped fracture and un-propped fracture exhibit different closure behavior during shut-in and early flowback periods corresponding to the dramatic change in effective stress, modeling of the realistic geometry and closure behavior of a partially-propped fracture is rarely performed when analyzing flow-back production data. In this study, geomechanical simulation is firstly used to simulate the closure behavior and to quantify the post-closure geometry of a partially-propped fracture. Then, results from the geomechanical simulation are incorporated into flow simulation to examine the impacts on recovery and distribution of fracturing fluid. At last, field data collected from two shale-gas wells in the Horn River Basin is analyzed to determine the potential implications of these uncertain factors on production forecast.

Geomechanical simulation based on explicit finite-difference method is used to simulate the change in effective stress and the corresponding geometry of a partially-propped fracture. Parameters including in-situ stress condition, proppant compaction, propped fracture aperture and secondary fractures are considered to understand their impacts on the post-closure geometry. This partially-propped fracture is then represented explicitly in the computational domain of a series of 3D flow numerical models, whose petrophysical parameters, fluid properties and operational constraints are representative of the Horn River shale gas deposits. The physical process of fracture closure is modeled by adjusting the fracture volume and fracture conductivity

dynamically. Non-Darcy behavior due to high gas velocity in fracture and matrix desorption are considered. The coupling of multi-phase flow, gravity and geomechanics is considered to examine the mechanisms responsible for the low fracturing fluid recovery and the ensuing fluid distribution away from the wellbore.

Geomechanial simulation confirms the formation of a residual opening above of the proppant pack in a partially-propped fracture. The size of this opening is most sensitive to the initial fracture aperture. Stress amplifies at the top of the proppant pack and leads to potential proppant crushing or embedment. Water uptake into the matrix is influenced by forced and spontaneous imbibition due to the large pressure differential across the matrix-fracture interface and matrix capillarity. Additional water is displaced into the matrix as pressure depletes and fracture closes. Gravity segregation may lead to water accumulating near the bottom of a vertical planar fracture, but fracture tortuosity could limit the segregation and promote a more uniform fluid distribution. Despite gas production is often hampered by non-uniform proppant distribution, the residual opening offers a highly conductive flow path for gas, which is much more mobile than the water-based fracturing fluid, further aggravating the phenomenon of gravity segregation. Therefore, more aggressive drawdown is recommended to flow back the fracturing fluid in the case of uneven proppant distribution. Extended shut-in time may enhance the initial gas rate, but lower late-time production is observed. The field case study suggests that considering these various physical mechanisms could improve the accuracy of the numerical model for history matching and the reliability of the ensuing production forecasting. Given that the solution to an inverse problem is generally non-unique, the results illustrate how additional uncertainty in production forecast is introduced when the scenario of non-uniform proppant distribution is ignored.

Dedication

To my ever loving and supportive parents, Weiming Liu and Lixin Liang

Acknowledgements

During my Master's study at the University of Alberta, I have gained so much assistance and support from many people. I would like to express my sincere acknowledgements to all of them, without whom this thesis would not have been possible.

First of all, I would like to express my sincere gratitude to my supervisors, Dr. Juliana Leung and Dr. Rick Chalaturnyk. I feel extremely fortunate to have the opportunity to study with them. I thank Dr. Rick Chalaturnyk for admitting me into his Reservoir Geomechanics Research Group (RG^2) and for his continuous generous support throughout my Master's study. The advice and freedom that he gave me, and his nice attitude are much appreciated. I learnt a lot of invaluable and applicable reservoir geomechanics knowledge from him. I thank Dr. Juliana Leung for her help and guidance when I was lost and helpless. Under her supervision, I got to know what research is, and how to do good research. I continuously gained from her insightful ideas and the discussions we had each week during the entire research. Whenever I encountered a problem, she always encouraged me with warm advice and guided me to the right track. She is such an ethical, professional and enthusiastic researcher that I feel honored to have this opportunity to work with her. She literally changed my life, turning a confused student into a potential researcher who even has the courage to pursue a doctorate degree. She deserves my sincere appreciation from the bottom of my heart.

I would like to thank my examining committee member, Dr. Hassan Dehghanpour, for his time, comments and valuable suggestions.

I would like to thank Dr. Clayton Deutsch and Dr. Samer Adeeb for their kindness and help in my Ph.D application. I also would like to thank Dr. Dave Chan and Arlene Figley for their kind help in dealing with the administrative issue.

My appreciation is extended towards my colleagues and friends at the University of Alberta for their direct or indirect help. In particular, I would like to thank Dr. Nathan Deisman, from the Reservoir Geomechanics Research Group, for his comments and fruitful discussions on the geomechanical modeling part of this research.

I am especially thankful for my good friend, Rencheng Dong from the University of Texas at Austin, who has shared a lot with me in the past years. I benefited a lot from our conversations. His encouragement and suggestions gave me hope and confidence to overcome some difficulties. I truly treasure our friendship.

The financial support provided by the Foundation CMG Industrial Research Consortia in Reservoir Geomechanics for Unconventional Resources, field data provided by Nexen ULC, and the academic licenses of CMG and FLAC2D respectively provided by Computer Modeling Group and Itasca Consulting Group, are all appreciated.

Finally, my greatest gratitude goes to my parents, to whom I owe everything in life, for their unconditional love, endless support and unwavering faith in me. I also would like to express my gratitude to my uncle, Baoheng Song who introduced me into the fascinating world of petroleum engineering, for sharing his life experience with me and for his continuous encouragement.

Table of Contents

List of Tables

List of Figures

Nomenclature

Symbols and abbreviations

ΔV = fracture volume change, m^3

a = fracture aperture, m

A = fracture area normal to the minimum horizontal stress, m^2

C_r = matrix compressibility, Pa^{-1}

E = Young's modulus, GPa

E^* = equivalent Young's modulus, GPa

F_{CD} = normalized fracture conductivity, dimensionless

G_s = gas content, gmol/kg

k = permeability, md

k_r = relative permeability

K = fracture conductivity, m^3

K_n = normal stiffness, GPa/m

P = fluid pressure, Pa

∇P = pressure drop, Pa

P_c = capillary pressure, Pa

P_i = initial reservoir pressure, Pa

P_L = Langmuir pressure, Pa

P_{wf} = bottom-hole pressure, Pa

s = natural fracture spacing, m

S_w = water saturation, dimensionless

SC = Surface condition

v = fluid velocity, m/s

V_L = Langmuir volume, gmol/kg

h = depth below the top of the reservoir

$Frac.$ = fracture

α = area contact ratio, dimensionless

β = non-Darcy coefficient, ft^{-1}

τ = tortuosity parameter, dimensionless

μ = fluid viscosity, Pa·s

ρ = density, kg/m^3

σ = interfacial tension between gas and water, N/m

σ_c = minimum in-situ stress, Pa

σ_c' = closure stress for hydraulic fracture, Pa

υ = Poisson's ratio, dimensionless

υ^* = equivalent Poisson's ration, dimensionless

φ = porosity, dimensionless

Subscripts

HF = hydraulic fracture

M = matrix

0 = initial state

t = tortuous fracture

g = gas phase

w = water phase

Chapter 1 Introduction

1.1 Background

The exploration and production of unconventional resources, including tight/shale oil/gas, coalbed methane, gas hydrate and heavy oil, have become more important with the ever increasing global demand for hydrocarbon resources (Zou 2012). And shale gas production accounts for a big portion of the total hydrocarbon production.

Shale gas reservoirs refer to non-buoyancy driven, continuous hydrocarbon plays that are composed of fine-grained sedimentary rocks, including true shales, mudrocks, limestones and siltstones (Chalmers et al. 2012; Gensterblum et al. 2015). Compared with conventional reservoirs, shale gas reservoirs are characterized by extremely low permeability and porosity. And capillary pressure in unconventional gas reservoirs can be very high due to its low permeability (Holditch 1979).

Horizontal drilling and multi-stage hydraulic fracturing are two key technologies in the economic development of unconventional tight/shale gas/oil reservoirs. Hydraulic fracturing technology can crack formation rocks through injecting fracturing fluid into reservoirs at high pressure and high rate, which can greatly increase the well productivity. The generic steps of hydraulic fracturing treatments can be divided into three phases: fracturing fluid injection period, shut-in (soaking) period and water recovery (flowback or cleanup) period (McClure 2014; Zhou 2016).

During the fracturing fluid injection phase, thousands of cubic meters of water along with proppants is pumped into the subsurface at high pressure (Holditch and Tschirhat 2005). Slick-

water is typically used as fracturing fluid in shale reservoirs (Mayerhofer and Meehan 1998). Water may leak off into matrix when fractures initiate and propagate during this period. However, the leak-off coefficient is pretty low in shale reservoirs due to its extremely low reservoir permeability (Wu et al. 2016). Hydraulic fractures may show some complexity and tortuosity due to the interaction with secondary fractures or weak interfaces in the reservoir (Fisher and Warpinski 2012). Fracture spacing is essential in the fracturing design, as the stress-shadow effects may severely reduce the fracturing effectiveness when the fracture spacing is small (Wheaton et al. 2014; Wu et al. 2016). The stress-shadow effects add additional compression on the interior fractures, resulting in severe growth restriction.

Prior to flowback, the well may be shut in for a number of operational reasons (Crafton and Noe 2013; Alkouh et al. 2014). During this period, fracturing fluid and gas redistribute in the fractured reservoir under complex interplay between capillarity and viscous force (Economides and Nolte 2000). Immediately following the injection phase, the fracture will close due to a drastic increase in effective stress acting on the fracture plane during the shut-in period and will further decrease in the subsequent flowback and production periods. Fracture closure is a complex multi-physics process, involving mechanical closure (McClure 2014, Shiozawa and McClure 2016a), multi-phase flow (Xu et al. 2016; Wang and Leung 2015) and proppant-rock interaction (Chen et al. 2015).

Flowback refers to the few hours or weeks of production immediately after shut-in period (Crafton 2010). However, many stimulated wells show surprisingly low fracturing fluid recoveries (Cheng 2012; Makhanov et al. 2014; Ghanbari and Dehghanpour 2016). Both field observations and numerical simulations indicate that the field operations, such as shut-in

duration and drawdown pressure, during flowback can influence the subsequent hydrocarbon production (Sherman and Holditch 1991; Crafton 2010; Fan et al. 2010; Cheng 2012; Wang and Leung 2015; Fakcharoenphol et al. 2013; Agrawal and Sharma 2015). However, no consistent conclusions are drawn.

1.2 Problem Statement

Based on various operational conditions, only 10% to 40% of the injected water-based fracturing fluid can be recovered during the flowback or cleanup period of the shale formations (Zhou 2016). The rest of the injected fluid remains in the fractured formation (King 2012). The unexpected low fracturing fluid recoveries raise several serious questions: what are the contributing factors controlling the fracturing fluid recovery? How does the fracturing fluid distribute in the fractured shale formation and how does it impact the well productivity?

In addition to matrix imbibition, fracture closure is another important mechanism that controls fracturing fluid recovery. The impacts of fracture closure can be complex: it leads to a reduction in fracture volume (aperture), which promotes water imbibition into the matrix during shut-in; on the other hand, it also causes fracture conductivity to drop, reducing fluid flow to the wellbore upon production. Therefore, the impact of physical process of fracture closure on fracturing fluid recovery and in-situ recovery should be investigated.

Besides, uniform proppant placement is a challenge in slick-water fracturing treatments because of the low viscous property of slick-water. Proppant distribution ultimately affects the fracture closure behavior and fracture conductivity. Closure of an un-propped fracture is controlled by the asperities of the fracture surface. Therefore, in a non-uniformly propped fracture, the different

response to effective stress change among the propped and un-propped sections may lead to a complex post-closure fracture geometry. The closure behavior and post-closure geometry of a partially-propped fracture, and their impacts on fracturing fluid flowback and subsequent gas production need to be investigated.

Water retention within the bottom of hydraulic fracture due to gravity segregation is another hypothesis. However, the tortuous nature of hydraulic fracture should affect the overall conductivity along the vertical direction, which may, in turn, influence the distribution of water and gas phases. Whether the water can permanently retain in the hydraulic fracture or slowly imbibe into matrix due to matrix capillarity is not clear. Thus, the recovery and in-situ distribution of fracturing fluid should be examined considering the effects of gravity and fracture tortuosity.

Furthermore, the flowback field operations can significantly affect the fracturing fluid recovery and subsequent gas production. The optimal operational strategy should be designed accounting for these physical mechanisms, including fracture closure, gravity segregation and proppant distribution.

1.3 Hypothesis

Uneven proppant distribution is often encountered in hydraulic fracturing. It is anticipated that the post-closure geometry of a partially-propped fracture is complex. Fluid dynamics within a partially-propped fracture with complex geometry must be different from that within a simple fracture with uniform properties. The contributions of the complex post-closure geometry of a

partially-propped fracture on recovery and in-situ distribution of fracturing fluid might be significant.

1.4 Research Objectives

The primary objective of this research is to study the coupling of fracture closure, gravity segregation and uneven proppant distribution in numerical simulation of fracturing fluid recovery and ensuing in-situ distribution. The overarching objective can be further divided into these components:

1. Model the post-closure geometry of a partially-propped fracture under realistic stress condition and rock properties using geomechanical simulation.

2. Incorporate fracture compaction and stress-dependent fracture conductivity into imbibition and flowback modelling.

3. Investigate the interplay between fracture closure, multi-phase flow and gravity segregation during shut-in and flowback.

4. Investigate the impacts of proppant distribution and post-closure geometry of a partially propped fracture on recovery and in-situ distribution of fracturing fluid, and subsequent gas production.

5. Discuss the implications and uncertainties if these complexities (e.g. fracture closure, proppant distribution) are ignored when analyzing flowback and production data through field case study.

Since practices for proper drawdown management and shut-in duration are still debatable among industry practitioners, this study will offer insights regarding fluid distribution mechanisms and optimization of operational design.

1.5 Thesis Outline

Chapter 1 presents the background related to this research including a brief introduction to shale gas reservoirs and hydraulic fracturing, problem statement and research objectives.

Chapter 2 presents a review of literature pertinent to mechanisms for low fracturing fluid recovery, and potential contributing factors controlling recovery and in-situ distribution of fracturing fluid. Drawbacks in existing numerical investigations of flowback are discussed.

Chapter 3 presents the methodology used in this study including geomechanical modeling of partially-propped fracture closure, and numerical simulation of multi-phase flowback and early-time production.

Chapter 4 presents the results of geomechanical simulation of partially-propped fracture closure. The post-closure geometry of a partially-propped fracture is quantified.

Chapter 5 presents the impacts of various factors on recovery and in-situ distribution of fracturing fluid. Insights pertinent to field operations are presented in this chapter as well.

Chapter 6 presents the results of field production data analysis. Implications and uncertainties if these complexities (e.g. fracture closure, proppant distribution, gravity) are ignored when analyzing flowback and production data are discussed.

Chapter 7 presents the key conclusions and recommendations for future work.

Chapter 2 Literature Review

2.1 Overview

In this chapter, literature relating to factors controlling recovery and in-situ distribution of fracturing fluid in unconventional reservoirs is reviewed. First, a review of the possible mechanisms for low fracturing fluid recovery is presented. This is followed by a review of previous investigations on hypothesized controlling factors (e.g. proppant distribution, fracture closure and gravity) responsible for low fracturing fluid recovery. At last, a review of existing relevant numerical studies is presented and some gaps in these existing studies are also discussed.

2.2 Mechanisms for Low Fracturing Fluid Recovery

A small portion of the injected fluid is recovered during the post-stimulation flow period or flowback (Abbasi et al. 2012; Abbasi et al. 2014). Numerous water-loss mechanisms and their impacts on subsequent well performance have been the subject of recent research efforts.

Water loss into reservoir matrix is one reason for low fracturing fluid recovery. Holditch (1979) studied the importance of capillarity and multi-phase flow effects for water recovery in low-permeability gas reservoirs with hydraulic fracturing. High capillary pressure and low water relative permeability can retain water in reservoir matrix over a long period of time, resulting in a low water recovery. This observation has also been confirmed by other studies (Wang et al. 2010; Gdanski and Walters 2010; Cheng 2012; Bertoncello et al. 2014; Wang and Leung 2015; Yue et al. 2016; Ghanbari and Dehghanpour 2016).

The injected fluid may also leak off into the surrounding natural or secondary fractures (Pagels et al. 2012; Fan et al. 2010). Cheng (2012) modeled a set of uniformly-distributed secondary fracture, which were fully connected to the main hydraulic fracture, and demonstrated that due to the enlarged fracture-matrix interface, more water may ultimately imbibe into matrix. Wang and Leung (2015) investigated the uncertainty in secondary fracture parameters with stochastic fracture networks. Their results indicated that if the water in the secondary fracture cannot be flown back due to insufficient drawdown, matrix imbibition will be important, even though it is a slow process. Based on those findings, we may conclude that the injected fluid may temporarily be trapped in the secondary fracture, but ultimately it either imbibes into matrix or flows back.

Water accumulation within the bottom of hydraulic fracture is another mechanism for low water recovery. In some cases, water retention within the hydraulic fracture may decrease the pressure differential between the hydraulic fracture and its surrounding matrix (Agrawal and Sharma 2015; Palisch et al. 2007). A schematic in **Figure 2-1** illustrates potential water distribution in a hydraulic fracture. Water loading or accumulation near the bottom has been observed in experimental (Parmar et al. 2012; 2013) and many numerical studies (Cheng 2012; Agrawal and Sharma 2015; Ghanbari and Dehghanpour 2016; Xu et al. 2016).

Geomechanics also plays a role in low water recovery because of fracture compaction and stress-dependent fracture conductivity during the shut-in and flowback periods (McClure 2014; Ehlig-Economides et al. 2012; Wang and Leung 2016). Proppant distribution ultimately affects the fracture closure behavior and fracture conductivity, which, in turn, affect the fracturing fluid recovery and in-situ distribution.

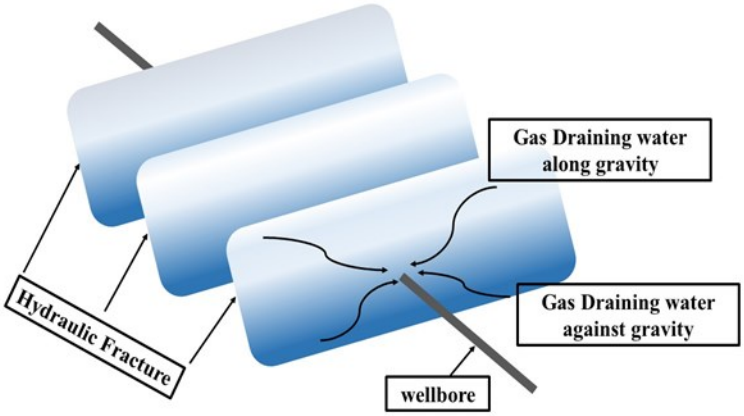

Figure 2-1 Schematic of water distribution in a hydraulic fracture (adapted from Agrawal and Sharma 2015)

2.3 Proppant Distribution in Hydraulic Fracture

Slick-water has been employed as the fracturing fluid extensively in unconventional reservoirs. Due to it much lower viscosity, as compared to a fully crosslinked gel (Palisch et al. 2010), an important concern with slick-water fracturing treatment is proppant transport/placement. Proppant placement entails not only the lateral placement along the fracture length, but also the vertical coverage across the fracture height. The vertical placement is of particular concern when the pay thickness is high (Palisch et al. 2010; Cipolla et al. 2009). Productivity of a hydraulic fracture is highly impacted by the proppant distribution (Daneshy 2005; Shah et al. 2001). Both analytical and experimental studies were conducted to examine proppant transport and placement in vertical fractures (Kern et al. 1959; Clark and Quadir 1981; Acharya 1986; Shah et al. 2001; Patankar et al. 2002). Although earlier studies focused on viscous or viscoelastic fracturing fluid,

such as gel, they highlighted the role of particle settling in proppant distribution. A typical proppant distribution in a vertical fracture is shown in **Figure 2-2**.

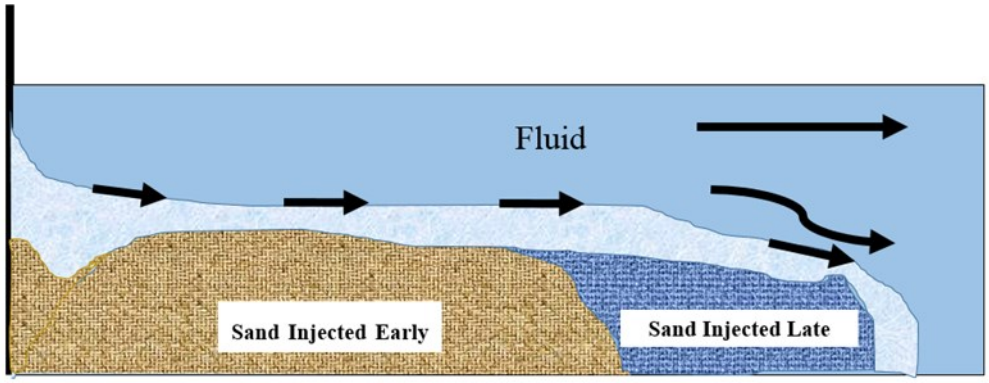

Figure 2-2 Schematic of proppant distribution in vertical fracture (adapted from Patankar et al. 2002)

More recent studies have focused on slick-water fracturing (Dayan et al. 2009; Sahai et al. 2014; Alotaibi and Miskimins 2015; Tong and Mohanty 2016; Shiozawa and McClure 2016b). Similar proppant settling in vertical fracture is observed in the experimental studies of Sahai et al. (2014) and Alotaibi and Miskimins (2015). Tong and Mohanty (2016) even included intersecting horizontal and vertical fractures in their experimental set-up. A numerical simulation based on the dense discrete phase model, which was also used by Zhang and Dunn-Norman (2015) and Deshpande et al. (2013), was constructed to predict the proppant settling. They reported three distinct zones across the vertical direction: an immobile sand bed in the bottom, a flowing slurry zone in the middle, and a clear fluid zone in the top. Similar conclusions were obtained using a 3-D hydraulic fracturing simulator with discrete fracture networks by Shiozawa and McClure (2016b). These studies highlight the importance of proppant settling, especially in low-

permeability formations, where fracture closes more slowly due to the low leak-off and allowing more time for particles to settle due to gravity.

2.4 Stress-Dependent Fracture Properties

Many studies have investigated the stress-dependent fracture properties (aperture and conductivity) through experiments conducted on fractured core plugs with or without proppant at different closure stress conditions (Fredd et al. 2001; Alramahi and Sundberg 2012; Cho et al. 2013; Huo et al. 2014; Zhang et al. 2014; Jansen et al. 2015; Kam et al. 2015). Closure stress refers to the effective stress acting on the fracture plane. The results confirmed that conductivity of the fracture decreases as the closure stress increases. And as expected, reduction in conductivity of an un-propped fracture is more prominent than that of a propped fracture (Zhang et al. 2014). Huo et al. (2014) explained that this reduction is the result of aperture reduction. Alramahi and Sundberg (2012) proposed a modified cubic relationship between normalized fracture conductivity and normalized fracture aperture at each closure stress to model this stress-dependent behavior.

Propped fracture and un-propped fracture exhibit different stress-dependent properties. Closure of an un-propped fracture is controlled by the asperities of the fracture surface, while the propped fracture closure is dependent on proppant properties. Therefore, in a partially-propped fracture, the different response to effective stress changes among the propped and un-propped sections may lead to a complex post-closure geometry. The hypothesized post-closure geometry of a partially-propped fracture is shown in **Figure 2-3**. Warpinski (2010) confirmed this hypothesis through analytical modeling. The fracture is identified into three regions: the propped region, the un-propped closed region and the residual opening (arch) on top of the proppant pack. Khanna et

al. (2014) modeled the residual opening using the distributed dislocation technique and concluded that the opening can act as a highly conductive pathway for fluid flow. Neto and Kotousov (2013) extended the work of Khanna et al. (2014) by incorporating proppant compaction. Their results indicate that the size of the residual opening and the associated degree of conductivity enhancement would depend on the system's mechanical properties, stress conditions and initial fracture geometry.

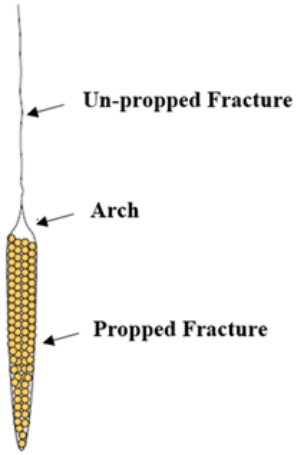

Figure 2-3 Schematic of fracture geometry after closure (adapted from Warpinski (2010))

2.5 Gaps in Existing Numerical Studies

The literature review in previous sections has indicated that gravity segregation, fracture tortuosity, fracture closure, and proppant distribution are potential contributing factors controlling the recovery and in-situ distribution of fracturing fluid, in addition to matrix capillarity. However these complexities are seldom accounted for in existing numerical investigations.

Water loading or accumulation near the bottom of the hydraulic fracture has been observed in the numerical studies of Cheng (2012), Agrawal and Sharma (2015), Ghanbari and Dehghanpour (2016) and Xu et al. (2016). They divided the hydraulic fracture into multiple layers in the vertical direction, but one important aspect is missing among these studies, which is the tortuosity of the hydraulic fracture (Warpinski et al. 2010; Fisher and Warpinski 2012). Mineback photograph confirms the complex, tortuous geometry of the hydraulic fracture due to the existence of secondary fractures or weak interfaces in the reservoir (Fisher and Warpinski 2012). It is anticipated that the tortuous nature of fractures should affect the overall conductivity along the vertical direction, which may, in turn, influence the distribution of water and gas phases.

Those experimental investigations mentioned in section 2.4 confirmed that fracture closes as effective stress acting on the fracture plane increases, which means that both the fracture conductivity and fracture aperture decrease as the closure stress increases. Many numerical studies have incorporated some elements of fracture closure in their numerical models (Huang and Ghassemi 2012; Yu and Sepehrnoori 2014; Wu et al. 2014; Wang et al. 2015); however, they generally ignored the explicit change in fracture volume as a result of fracture aperture reduction. For example, only stress-dependent fracture conductivity was incorporated into the numerical models of Wang et al. (2010), Cheng (2012), and Wang and Leung (2016) to account for the impacts of fracture closure on fracturing fluid flowback or cleanup. However, Ezulike et al. (2016) stated that fracture volume reduction plays an important role during early-flowback depletion. Their analytical volumetric analysis indicated that ignoring the fracture volume changes during reservoir depletion could lead to misleading history matching and erroneous

forecasting when applied to field data. Even though Wang and Aryana (2016) presented a numerical model that also incorporated fracture aperture reduction, but the flow is single-phase in their study and the specific impacts on fracturing fluid recovery and in-situ distribution were not addressed. Therefore, further numerical studies are needed to incorporate detailed modeling of fracture closure when examining fluid distribution at different stages of production (e.g. shut-in, flowback and post-flowback periods).

Another issue needed to be addressed is the impacts of proppant distribution. Although abundant studies have confirmed that uniform proppant distribution is challenging in slick-water fracturing treatments, only a few numerical studies incorporate non-uniform proppant distribution in their models. Zanganeh et al. (2015) utilized a fracture propagation simulator to generate a partially-propped fracture, which was subsequently subjected to two-phase flow simulation for a tight oil reservoir; however, capillarity was ignored, and the difference in closure behavior and stress-dependent conductivity between the propped and un-propped sections were not considered. Again, proppant distribution ultimately affects the fracture closure behavior and post-closure geometry (Warpinski 2010). However, this residual opening is generally ignored in most geomechanical modeling studies involving partially-propped fracture, such as Shiozawa and McClure (2016b), as well as other studies that investigated the impact of non-uniform proppant distribution on well productivity, such as Sierra et al. (2014). Both of these two studies just classified the whole hydraulic fracture into two regions: propped fracture and un-propped fracture. The arch region formed above the proppant pack has extremely high conductivity, which should have a significant impact on flowback and production (Warpinski 2010). For example, Cipolla et al. (2009) investigated the impact of this residual opening on gas production

through numerical simulations and they concluded that this opening would enhance gas production and reduce the requirement for fracture conductivity to achieve economic production. However, in this study, multi-phase flow and fracture closure were not included. Therefore, the closure behavior and post-closure geometry of a partially-propped fracture need to be examined by geomechanical modeling. And numerical models investigating mechanisms controlling fracturing fluid flowback efficiency should incorporate these complexities.

Insights from various previous studies about fluid distribution and optimal field operational strategy, such as shut-in and drawdown pressure, are not consistent. Sherman and Holditch (1991) indicated that low fracturing fluid recovery would have a negative effect on gas production. A less aggressive drawdown was recommended to reduce closure stress and to enhance fracture conductivity. However, gravity segregation is ignored in their 2-D models. Wang et al. (2010) indicated that ignoring gravity effects (and the associated water blockage) would underestimate effective fracture conductivity. They recommended operating with a bottom-hole pressure of 10% of initial reservoir pressure to mitigate liquid loading. Agrawal and Sharma (2015), however, argued that high drawdown would enhance fracturing fluid recovery in dry gas recovery, but stress-dependent fracture properties was not incorporated. The benefits of larger drawdown may be counteracted by the reduction of fracture conductivity.

Other studies, including Cheng (2012) and Ghabari and Dehghanpour (2016), encouraged extended shut-in to promote initial high gas production. Because the field data from a shale gas reservoir in the Horn River Basin indicated that higher initial gas production always associates with lower fracturing fluid recovery (Ghabari and Dehghanpour 2016), and the initial gas rate of a well from Marcellus formation was significantly enhanced after a shut-in period (Cheng 2012).

Fan et al. (2010) also stated that wells with less flowback water have better early production rates. However, Wang and Leung (2015) argued that prolonged shut-in has minimal impact on long-term production. Similar findings were reported in Fakcharoenphol et al. (2013). And Crafton and Noe (2013) even concluded that extended shut-in duration can be detrimental to well performance. Therefore, optimal field flowback operation should be further examined accounting for more physical mechanisms, such as fracture closure, proppant distribution, post-closure geometry of a partially-propped fracture, and gravity segregation.

In summary, the literature review has identified a few gaps in existing numerical modeling studies involving flowback analysis. In particular, incorporating realistic post-closure geometry of a partially-propped fracture and its subsequent closure are needed. Physical process of fracture closure should be captured by modelling both fracture aperture and conductivity changes as a function of closure stress, instead of just modeling fracture conductivity changes. More analysis that couples gravity, multi-phase flow and geomechanics, especially in the case of a partially-propped fracture, is needed to understand fracturing fluid recovery and ensuing in-situ distribution. Insights regarding fluid distribution mechanisms and optimization of operational design should be offered based on models accounting for more complex mechanisms discussed in this chapter.

Chapter 3 Methodology

3.1 Overview

The methodology used in this study is presented in this chapter. Firstly, geomechanical simulation based on explicit finite-difference method is used to simulate the change in effective stress and the corresponding geometry of a partially-propped fracture. Parameters including rock strength, in-situ stress condition, proppant compaction, propped fracture height and aperture are considered to understand their impacts on the resultant fracture geometry through sensitivity analysis. Then, a series of 3D flow simulations are conducted to model multi-phase fluid flow during the shut-in, flowback and early post-flowback periods. The numerical models are constructed based on petrophysical parameters, fluid properties and operational constraints representative of Horn River shale gas reservoir. The partially-propped fracture is represented explicitly in the computational domain. Fracture volume and conductivity are adjusted dynamically to model the physical process of fracture closure.

3.2 Geomechanical Modeling of Partially-Propped Fracture Closure

Explicit finite-difference mechanics computations are performed using FLAC2D (Itasca 2015) to simulate the change in effective stress and the corresponding deformation in a partially-propped fracture. The objective is to assess its closure behavior and post-closure geometry.

A 6 m × 50 m model is constructed. It is assumed that a two-dimensional planar fracture that is 40m in height is placed at the center of the model. Two-dimensional planar fracture is modeled because fracture is assumed to propagate along the direction of maximum horizontal stress;

hence, fracture aperture variation is ignored. The bottom half of the fracture is filled with proppants (i.e., propped), while the upper half is empty (i.e., un-propped) (**Figure 3-1**). Relevant geomechanical properties, stress and pore pressure conditions are extracted from Chou et al. (2011) and Novlesky et al. (2011), and they are summarized in **Table 3-1**. It is assumed that the rock exhibits linear elasticity and the normal vector of the fracture plane is parallel to the minimum horizontal stress, which is approximately 55 MPa based on a stress gradient of 22 kPa/m and a reservoir depth of 2500 m. The simulation process is schematically illustrated in **Figure 3-2**. The initial fracture pressure (t = 0) is equal to the minimum horizontal stress to model the reservoir condition immediately following the injection of hydraulic fracturing fluid. Once the injection stops, the pressure inside the fracture gradually decreases (t > 0), and fracture starts to close until the equilibrium condition is achieved. Constant total stress is applied at the boundary.

Table 3-1 Geomechanical properties used in this study

Min. Horizontal Stress Gradient	Pore Pressure Gradient	Bulk Density	Young's Modulus	Poisson's Ratio
22 kPa/m	12.5~14.5 kPa/m	2600 kg/m^3	29 GPa	0.2

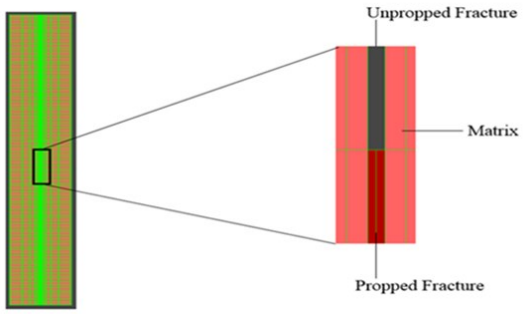

Figure 3-1 Geomechanical model of a partially-propped fracture

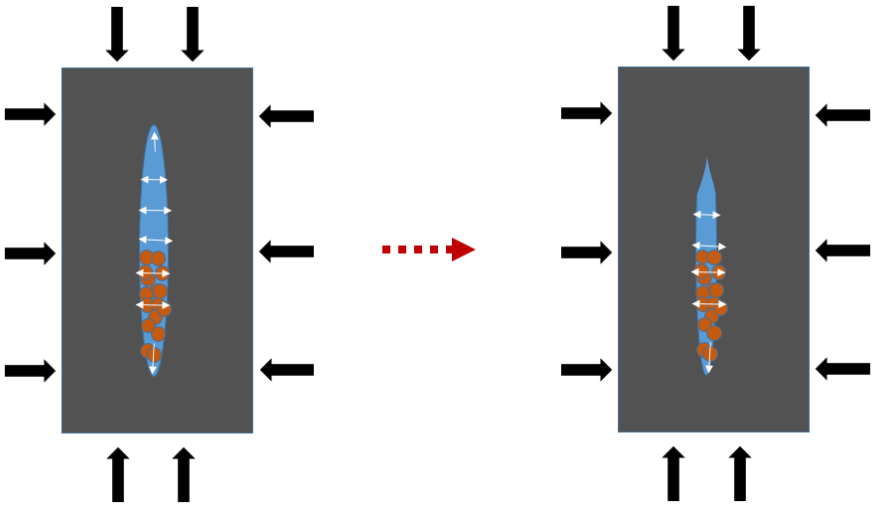

Figure 3-2 Schematic of geomechanical simulation process. Black arrows represent boundary stress; white arrows represent fracture pressure.

The simulation results reveal that three distinct regions may exist within the fracture upon closure: a propped region, an un-propped closed region and a residual opening (arch). To incorporate the effects of secondary (natural) fractures in shale matrix, the matrix is represented as a rock mass consisting of laminations or weak planes, resulting in transversely isotropic properties. An equivalent continuum model, proposed by Amadei and Goodman (1981), is adopted to upscale a transversely isotropic fractured medium into an equivalent elastic anisotropic continuum medium (Gu and Chalaturnyk 2010). The equivalent Young's modulus and equivalent Poisson's ratio in the direction orthogonal to the weak planes are calculated according to **Eqs. 1-2**:

$$\frac{1}{E^*} = \frac{1}{E} + \frac{1}{K_n \cdot s} \quad \text{.....(1)}$$

$$\nu^* = \frac{E^*}{E}\nu \quad \text{.....(2)}$$

E and ν are the Young's Modulus and Poisson's ratio of the intact rock, respectively. The superscript (*) denotes an equivalent continuum media consisting of secondary fractures; s represents the secondary fracture spacing, and K_n is the normal stiffness of the secondary fracture. It is clear that rock strength is weakened in the presence of secondary fractures. Propped fracture compaction as a result of proppant deformation (e.g., embedment and crushing) is modeled by assigning softened properties inside the fracture. Parameters including rock strength, in-situ stress condition, proppant compaction, propped fracture height and aperture are investigated to understand their impacts on the resultant geometry by sensitivity analysis.

3.3 Multi-Phase Flow Simulation

A set of 3D compositional simulation models (210 m × 510m × 115m) is constructed using GEM (CMG 2015). The grid consists of 51 × 55 × 15 cells with a total of 15 layers along the vertical direction. The grid is locally refined around the well and the hydraulic fracture. Relevant reservoir, fluid and well parameters are extracted from representative values for the Horn River shale reservoirs (Nejadi et al. 2015; Anderson et al. 2013; Novlesky et al. 2011), as summarized in **Table 3-2.** Although uneven proppant distribution and heterogeneous fracture properties along the vertical direction are modeled, hydraulic fracture stages are assumed to be evenly spaced and symmetrical; thus, only one stage is simulated. The top view of the simulation model is shown in

Figure 3-3. The well perforation is located at the intersection of the hydraulic fracture and the horizontal well.

Table 3-2 Summary of reservoir, well and fluid properties for flow simulation models

Parameters	Value
Initial reservoir pressure P_i	3.2×10^7 Pa
Initial fracture pressure P_{fi}	5.5×10^7 Pa
Minimum wellbore flowing pressure P_{wf}	1.0×10^7 Pa
Rock compressibility C_t	2.5×10^{-9} Pa^{-1}
Matrix permeability k_M	0.2×10^{-18} m^2
Matrix porosity ϕ_M	0.06
Hydraulic-fracture porosity ϕ_{HF}	1
Matrix initial water saturation S_{wM}	0.25
Hydraulic-fracture initial water saturation	1
Initial hydraulic-fracture aperture	0.02 m

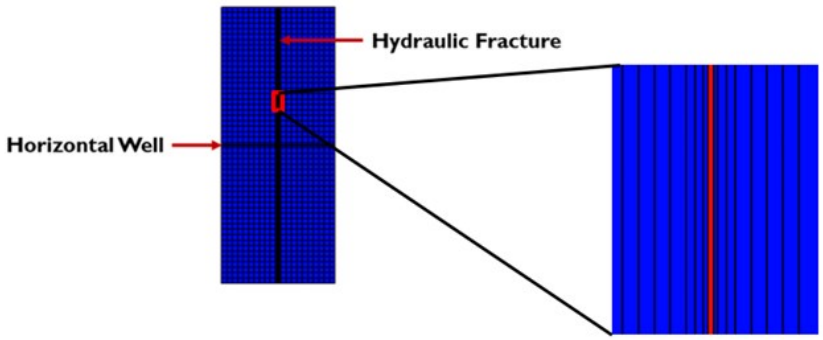

Figure 3-3 Top view of numerical simulation model for flow simulation

The Langmuir isotherm in **Eq. 3** is adopted to model the amount of adsorbed gas on the shale matrix (G_s) as a function of pressure (P) (Langmuir, 1918). The Langmuir constants are assigned based on the experimental measurement of Novlesky et al. (2011), where V_L = 0.128 gmol/kg and P_L = 6451.6 kPa.

$$G_s = \frac{V_L P}{P + P_L} \quad \text{..... (3)}$$

3.3.1 Relative Permeability and Capillary Pressure Functions

Separate water-gas relative permeability function is assigned to hydraulic fracture and matrix respectively, as shown in **Table 3-3.** It is assumed that capillary pressure in hydraulic fracture is negligible due to its high conductivity, while capillary pressure in the matrix is modeled using **Eq. 4**, an empirical relationship proposed by Gdanski et al. (2009) that is based on the "Leverett J-function" (Leverett 1941).

$$P_c = \frac{\sigma}{a_2 (S_w)^{a_1}} \left(\frac{\varphi}{k}\right)^{a_3} \times 6894.76 \quad \text{..... (4)}$$

Interfacial tension (σ) between gas and water is 40 dynes/cm. The constants, a_1 = 1.86 and a_2 = 6.42, are representative of the low-permeability reservoirs (Gdanski et al. 2009; Holditch 1979); a_3 is a measure of pore structure, and it is set to be 0.5 (Bradley 1992; Wang and Leung 2015). Non-Darcy flow effect due to high-velocity turbulent gas flow in the hydraulic fracture is modeled using the Forchheimer modification and Darcy's Law in **Eq. 5**:

$$-\nabla P = \frac{\mu}{k} v + \beta \rho v^2 \quad \text{..... (5)}$$

where v is velocity, μ is viscosity, k is permeability, ρ is density. The constant β is determined using **Eq. 6**, which was an empirical correlation proposed by Evans and Civan (1994), who analyzed 180 experimental measurements of propped fracture properties. In **Eq. 6,** the unit of permeability k is md and unit of β is ft^{-1}.

$$\beta = \frac{1.485e^{9}}{k^{1.021}} \quad \text{..... (6)}$$

A tortuosity parameter (τ) is defined according to Chen et al. (2015) to represent the ratio of the length of the actual flow path to the direct distance between two cross-sections for fluid flow. Tortuosity negatively impacts the fracture conductivity, and this is accounted for with a modified tortuous fracture conductivity (K_t) according to **Eq. 7**, where K is the conductivity of a planar fracture with $\tau = 1$.

$$K_t = \frac{1}{\tau} K \quad \text{..... (7)}$$

Table 3-3 Relative permeability functions of matrix and hydraulic fracture

Matrix				**Hydraulic Fracture**		
S_w	k_{rw}	k_{rg}		S_w	k_{rw}	k_{rg}
0.25	0.0	0.9		0	0	1
0.319	0.00078	0.60293		0.125	0.125	0.875
0.353	0.00264	0.48274		0.250	0.25	0.75
0.388	0.00625	0.37969		0.313	0.3125	0.6875
0.422	0.01221	0.29246		0.375	0.375	0.625
0.456	0.02109	0.21973		0.438	0.4375	0.5625
0.491	0.03350	0.16018		0.500	0.5	0.5
0.525	0.05000	0.11250		0.563	0.5625	0.4375
0.559	0.07119	0.07537		0.625	0.625	0.375
0.628	0.12998	0.02747		0.750	0.75	0.25
0.697	0.21455	0.00593		0.813	0.8125	0.1875
0.731	0.26797	0.00176		0.875	0.875	0.125
0.766	0.32959	0.00022		0.938	0.9375	0.0625
0.80	0.4	0.00		1.000	1	0

3.3.2 Model Initialization

There are various approaches for simulating the hydraulic fracturing process. A common strategy is to incorporate an injection phase to model fluid leak-off during the hydraulic fracturing treatment (Agrawal and Sharma 2015; Gdanski et al. 2009; Alkouh et al. 2014; Ghanbari and Dehghanpour 2016; Wang and Leung 2016). Despite ignoring the propagation of fracture, this approach would simulate certain degree of fluid leak-off prior to the shut-in stage. However, an inconsistency is that, in those studies, the initial hydraulic fracture porosity was set to be less than one, representing some post-closure state; hence, fracture closure due to change in effective stress was not considered explicitly. An alternative approach is adopted in this study: the initial pressure inside the hydraulic fracture is equal to the minimum horizontal stress, in order to model the reservoir condition immediately following the injection of hydraulic fracturing fluid. The fracture is assumed to be completely open with an initial porosity of one. No injection period is modeled, so fluid leak-off during the fracture propagation stage is ignored. This simplification seems appropriate considering that the leak-off coefficient (in the order of 0.00001 $ft/min^{0.5}$) is generally quite small in most unconventional tight/shale reservoirs (Wu and Olson, 2016; Shiozawa and McClure 2016b). However, during the shut-in and subsequent flowback/production periods, the fracture will close, allowing fluid that is initially inside this open fracture to flow into the surrounding matrix.

3.3.3 Modeling of Fracture Closure

Once the fluid injection phase has ceased, fracture will close abruptly due to a drastic increase in effective stress acting on the fracture plane. To represent this closure process, both fracture

volume and conductivity are adjusted as a function of effective stress, assuming that the total in-situ stress is constant. Based on the geomechanical modeling in section 3.2, three distinct regions with different closure behavior are represented in the computational domain explicitly to model the propped, un-propped and residual opening portions of a partially-propped fracture.

First, variation in fracture conductivity with effective stress is modeled after experimental measurements conducted by Kam et al. (2015) on shale cores extracted from the Horn River formation at reservoir conditions, as shown in **Figure 3-5**. Their results suggest that irrespective to the proppant distribution, fracture conductivity declines more quickly at low closure stress, since fracture surface stiffness increases with closure stress (Fredd et al. 2001; Alramahi and Sundberg 2012). It is assumed that the total stress acting on hydraulic fracture is equal to a constant in-situ minimum horizontal stress (σ_c), and the closure stress (σ_c') is computed using the Terzaghi's effective stress equation in **Eq. 8**.

$$\sigma_C' = \sigma_C - P_{HF} \quad \text{..... (8)}$$

To facilitate updating the fracture property at each time step, a fracture conductivity multiplier or F_{CD}, which is the defined as the fracture conductivity at a given closure stress normalized against its value at the initial closure stress, as a function of fluid pressure in the fracture (P_{HF}) is derived from **Figure 3-4**, and the result is shown in **Figure 3-5**. The "propped" relationship is also used to model the closure of the residual opening portion.

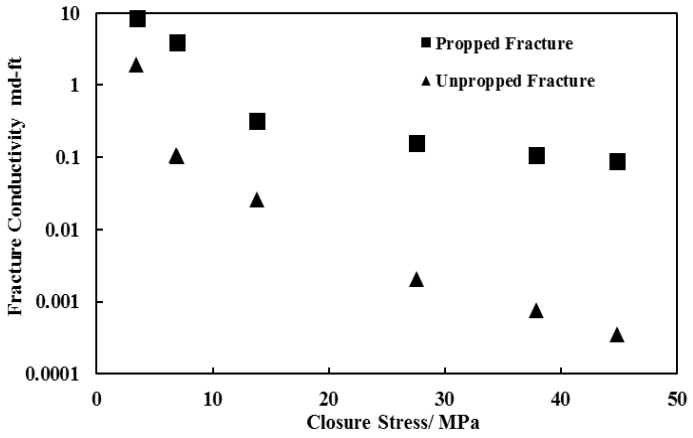

Figure 3-4 Measurements of hydraulic fracture conductivity at different closure stress for Horn River shale cores (adapt from Kam et al. 2015)

Next, to compute the change in fracture volume with closure stress, it is assumed that the fracture area normal to the minimum horizontal stress (A) remains constant. As a result, aperture (a) is related to the conductivity (K) following the modified cubic law or **Eq. 9**, which was developed by Alramahi and Sundberg (2012) based on experimental data.

$$K = \frac{1-\alpha}{1+\alpha}\frac{16a^3}{3\mu} \quad \text{..... (9)}$$

Combining the definition of F_{CD} and **Eq. 9** would yield **Eq. 10** for constant contact area ratio (α).

$$F_{CD} = \frac{K}{K_0} = \left(\frac{a}{a_0}\right)^3 \quad \text{..... (10)}$$

To avoid modifying the width of the fracture cell dynamically, the change of fracture aperture can be realized by adjusting the fracture porosity to achieve an equivalent reduction in fracture volume according to **Eq. 11**.

$$\Delta V = A\left(a_0 - a\right)\phi_0 = Aa_0(\phi_0 - \phi) \quad \text{..... (11)}$$

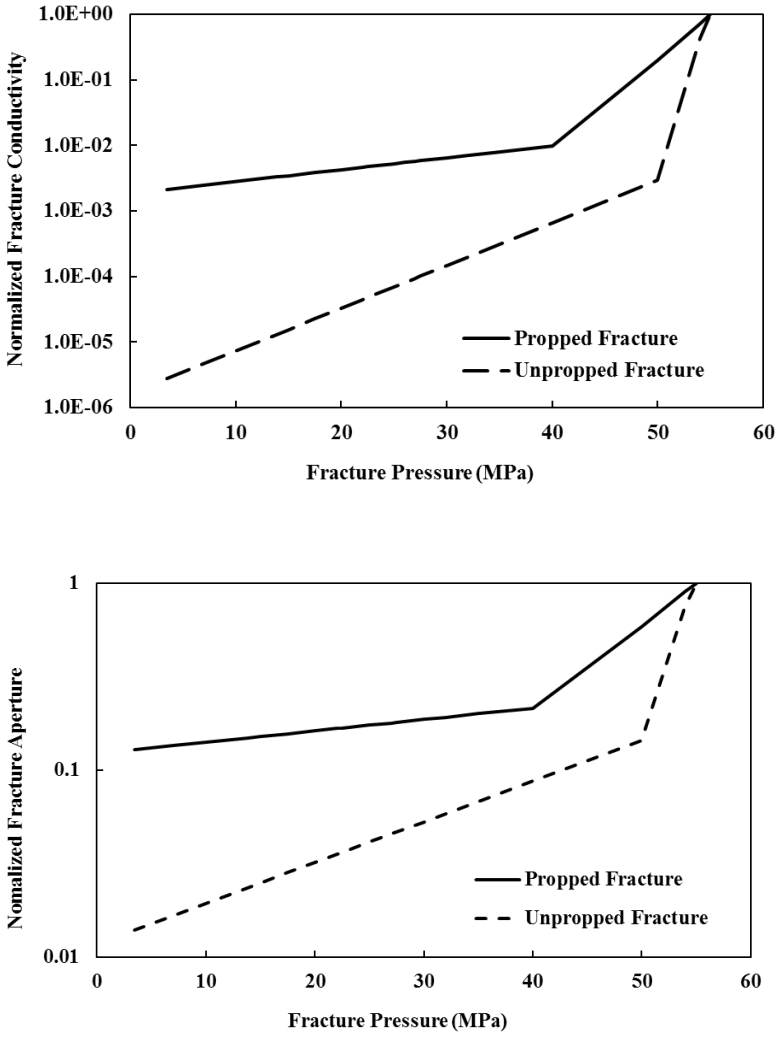

Figure 3-5 Normalized fracture conductivity (F_{CD}) and aperture as a function of fluid pressure inside fracture

3.4 Assumptions

This section lists the assumptions that are made in this modeling study. For the geomechanical simulation part, the main assumptions are:

1. The rock exhibits linear elasticity and the normal vector of the fracture plane is parallel to the minimum horizontal stress.

2. The proppant distribution is assumed uneven only in the vertical direction, so only the post-closure geometry in the vertical direction is modeled using a 2-D model.

3. Poromechanical effect is not considered in the geomechanical simulations. The fracture pressure is modeled by assigning internal force on the interfaces, and is decreased at each time step.

For the flow simulation part, the main assumptions are:

1. Planar hydraulic fracture is assumed, although the fracture tortuosity is modeled by introducing a parameter defined by the ratio of actual flow path to direct flow path between two cross-sections for fluid flow.

2. Fracturing fluid leak-off during the fracture propagation stage is ignored, considering its small volume compared with that during the shut-in period.

3. The complexities induced by the existence of natural fractures, such as the effects on multi-phase flow functions, initial fluid saturations and geochemical interactions, are beyond of the scope of this research. Instead, this research is focused on the impacts of heterogeneous hydraulic fracture properties.

Chapter 4 Analysis of Post-Closure Geometry of a Partially-Propped Fracture

4.1 Overview

The results of geomechanical simulation of partially-propped fracture closure are summarized in this chapter. The changes in effective stress and the corresponding post-closure geometry of a partially-propped fracture are presented. The impacts of secondary fractures, in-situ stress condition, proppant compaction, propped fracture height and aperture on the resultant geometry are discussed through sensitivity analysis.

4.2 Quantitative Description of Post-Closure Geometry

Results of the geomechanical simulation are compared qualitatively against an analytical model in Warpinski (2010). In both models, proppant compaction is ignored. Similar fracture geometry during closure is observed. Simulation results comparing the initial and final fracture geometry for the base case (a = 0.02 m) after closure is shown in **Figure 4-1**. The result confirms the formation of a residual opening above of the proppant pack in a partially-propped fracture. Three distinct parts are identified within a partially-propped fracture: a propped region, an un-propped closed region and a residual opening (arch). The arch is triangular in shape, and its size can be represented by an equivalent height, which is obtained by dividing its cross-sectional area by the final post-closure aperture of the propped segment. This equivalent height is in the same order of magnitude as the value estimated from the analytical model (Warpinski 2010).

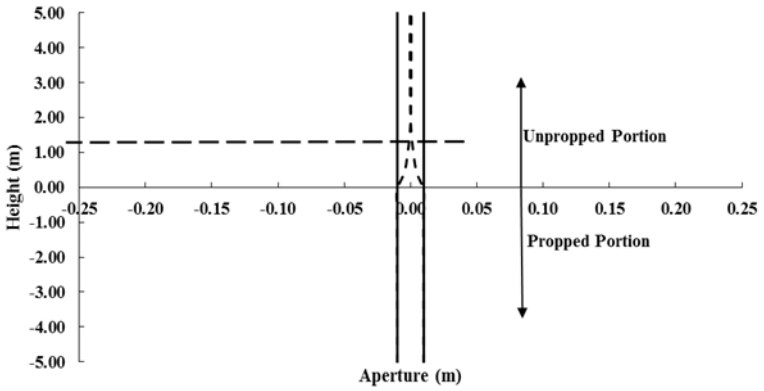

Figure 4-1 Comparison of initial and final (post-closure) geometry for a partially-propped fracture with initial aperture of 0.02 m

4.3 Sensitivity Analysis

It is hypothesized that the size of this residual opening is most sensitive to the initial fracture aperture. Firstly, a series of sensitivity analysis is conducted by varying the initial aperture between 0.005 m and 0.05 m (capturing the range of values typically encountered in the field), and the corresponding fracture geometries after closure are shown in **Figure 4-2**. The equivalent height of the residual opening as a function of initial fracture aperture obtained from these geomechanical simulations is shown in **Figure 4-3**. The height of the arch increases as the initial fracture aperture increases.

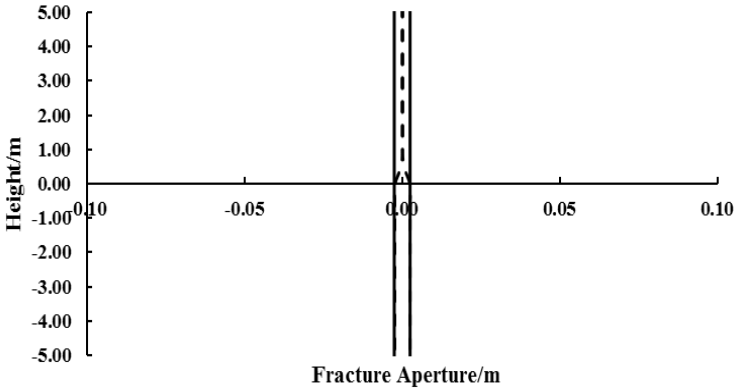

***a* = 0.005 m**

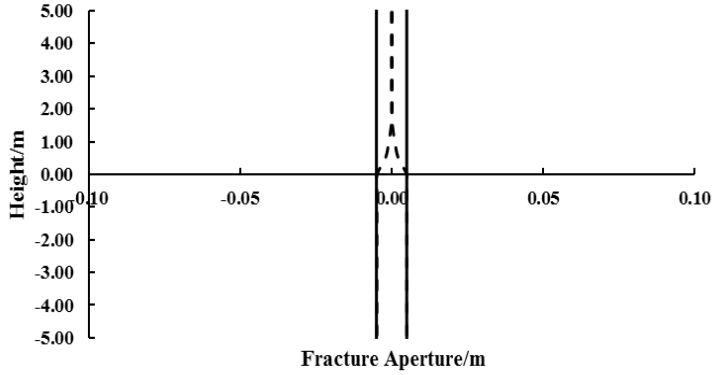

***a* = 0.01 m**

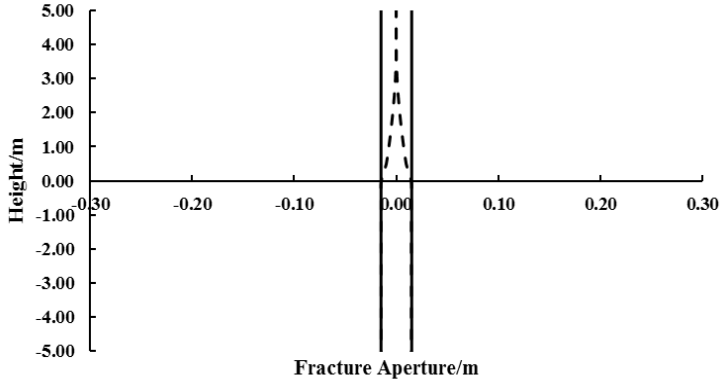

***a* = 0.03 m**

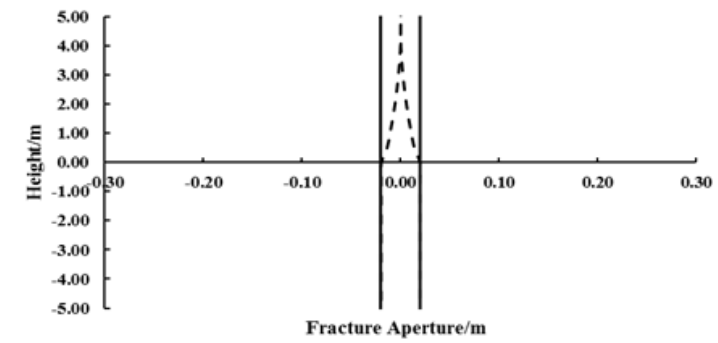

***a* = 0.04 m**

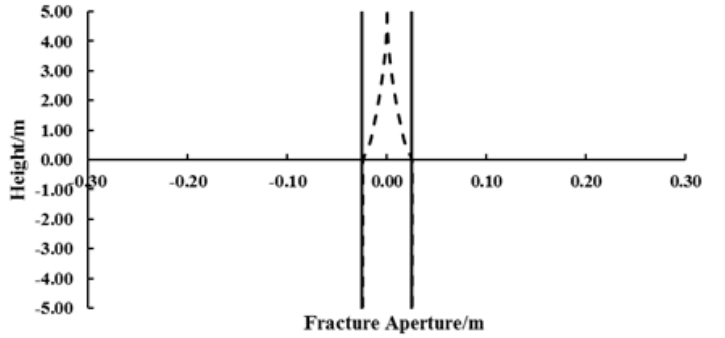

***a* = 0.05 m**

Figure 4-2 Comparison of initial and final (post-closure) geometry for a partially-propped fracture with different initial aperture (a)

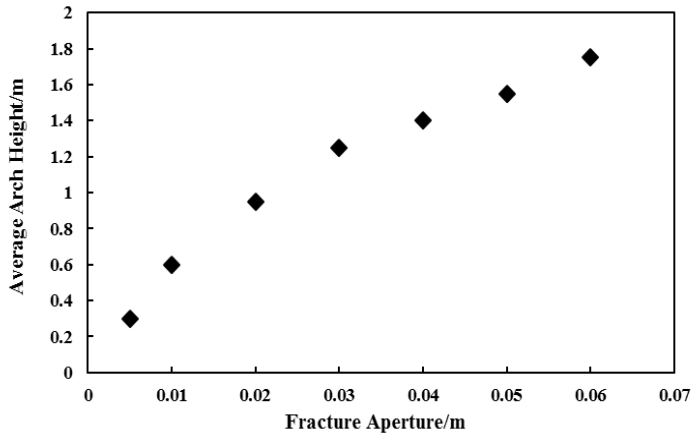

Figure 4-3 Equivalent arch height as a function of initial fracture aperture

Then, sensitivity analysis on in-situ conditions is conducted. In additional to the base case with stress ratio of 1, cases with higher stress ratio of 1.2 and 1.4 are simulated by increasing the overburden stress. In 2D, stress ratio is defined as the ratio of overburden stress to minimum horizontal stress. There is no observable difference in the post-closure geometry. This observation is reasonable considering the minimum horizontal stress, which also represents the normal stress acting on the fracture plane, is the dominant parameter. A similar observation is obtained when secondary fractures are present. Using K_n = 50 GPa/m and s = 2 m, E^* and ν^* are reduced to 22.5 GPa and 0.16 from the original E and ν values of 29 GPa and 0.2, respectively. It was noted that the post-closure geometry is only slightly affected. Results of this sensitivity analysis would suggest that anisotropic stress state and presence of secondary fractures are not important factors in controlling the post-closure geometry of a partially-propped fracture.

Lastly, the proppant compaction is modeled. The results indicate that more severe deformation is observed at the top of the propped section (**Figure 4-4**), and this may result in potential proppant

embedment or crushing. In addition, stress amplification ratio is defined as the stress acting on the proppant pack after closure divided by its value prior to closure. It is shown as a function of vertical distance away from the top of the proppant pack along the fracture plane for the base case with initial fracture aperture of 0.02 m in **Figure 4-5**. It is clear that the stress amplification is the highest at the top of the propped fracture, since the proppant must support the fracture, as well as the residual opening that is located right on top (Warpinski 2010; Neto and Kotousov 2013).

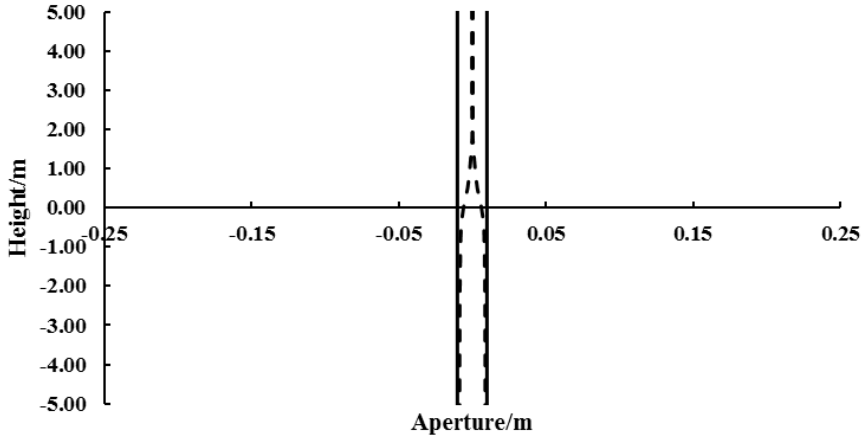

Figure 4-4 Comparison of initial and final (post-closure) geometry for a partially-propped fracture with considering proppant compaction

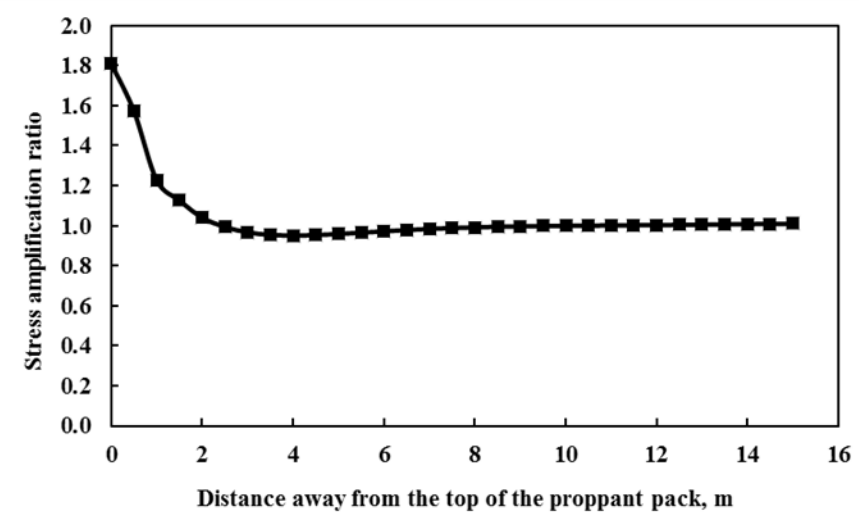

Figure 4-5 Stress amplification ratio as a function of the vertical distance away from the top of proppant pack along the fracture plane.

4.4 Summary

Geomechanical simulations presented in this chapter confirm the complex post-closure geometry of a partially-propped fracture. Three distinct parts are identified within a partially-propped fracture: a propped region, an un-propped region and a residual opening (arch). The size of this opening is most sensitive to the initial fracture aperture. Stress amplifies at the top of the proppant pack and leads to potential proppant crushing or embedment. A further hypothesis is that this complex post-closure fracture geometry would have some impacts on the multi-phase fluid flow, especially the highly conductive residual opening. Thus, in the following chapters, numerical investigations and field production data analysis will be conducted to examine it impacts on multi-phase fluid flow.

Chapter 5 Simulation of Recovery and In-situ Distribution of Fracturing Fluid

5.1 Overview

In this chapter, flow simulation models are constructed to model fluid distribution during shut-in, flowback and production periods. The coupling of multi-phase flow, gravity and geomechanics is simulated to examine the mechanisms responsible for the low fracturing fluid recovery and the ensuing fluid distribution away from the wellbore. First, modeling of the fracture closure process is discussed. Next, factors that may influence fluid distribution and recovery, such as gravity segregation, fracture tortuosity, proppant distribution and post-closure fracture geometry, are examined. In non-uniform proppant distribution scenario, three distinct regions corresponding to the propped, un-propped and residual opening portions are assigned based on the geomechanical simulation results of the base case in Chapter 4. Finally, impacts of some operational parameters, such as drawdown and shut-in duration are systematically investigated.

5.2 Fracture Closure

Reduction in fracture volume is often ignored in numerical simulations when modeling fracture closure. In this section, the method outlined in section 3.3.3 is followed to model the change in fracture volume (aperture/porosity) and conductivity with effective stress. It is clear from **Figure 5-1** that when fracture volume change is ignored, the model overestimates the total water recovery by approximately 40%. Capillary end effect or fracture face effect characterized by a jump in saturation is observed at the matrix-fracture interface, where there is a discontinuity in

capillary pressure across the interface. In both models, the proppant distribution is assumed to be uniform. It is interesting to note that if the reduction in fracture volume is modeled, though the final recovery is lower, the initial water recovery is higher during the early production or flowback stage. This is because, during the shut-in period, decreasing fracture volume has driven more water to imbibe into matrix. This is also confirmed by the higher water saturation in the matrix near the fracture interface.

This comparison highlights the critical role of fracture volume reduction in controlling the fracturing fluid recovery and distribution. Therefore, the base case for the subsequent sections will incorporate reduction in both conductivity and volume during fracture closure.

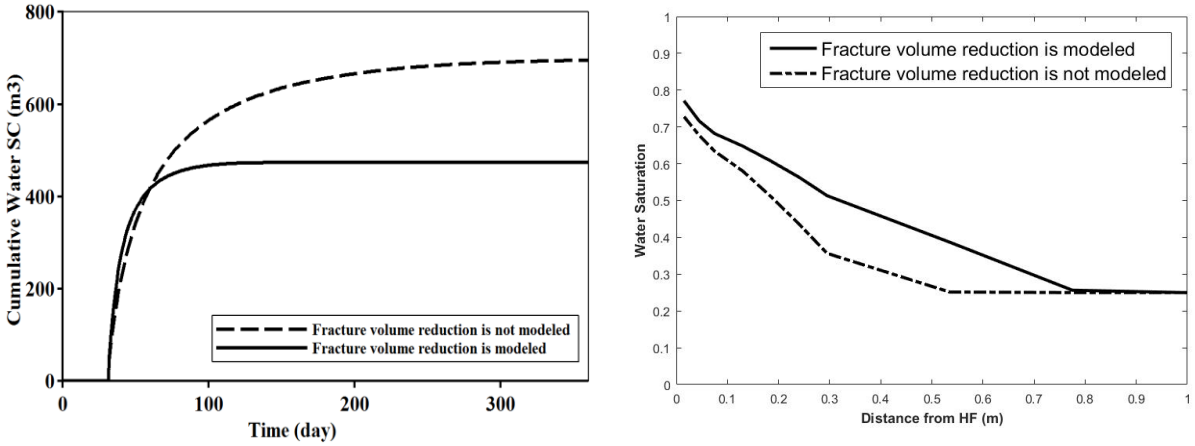

Figure 5-1 Comparison of cumulative water production or total water recovery (top) and the average water saturation as a function of distance away from the fracture-matrix interface (bottom)

5.3 Gravity Segregation and Fracture Tortuosity

To assess the sensitivity in fracturing fluid recovery and distribution due to gravity segregation, a few case studies are constructed. The base case is constructed using the parameters described in Chapter 3, assuming uniform proppant distribution. Another scenario (Case 1) is constructed by assigning a single layer along the vertical direction. Water saturation inside the hydraulic fracture plane at various depths is plotted as a function of time during the shut-in period in **Figure 5-2**. It is obvious that for the base case, water saturation remains close to one near the bottom after 31 days of shut-in; on the other hand, layer 1, which is located at the top, is almost fully saturated with gas. To further investigate the gravity effects, **Figure 5-3** shows the water saturation profile as a function of time in layer 15 (the bottom of the hydraulic fracture for the base case). After the entire one-month shut-in period has concluded, it is completely saturated with water. During the early-flowback or initial production stage, the water saturation has decreased very slowly. After the water near the top of the hydraulic fracture has been flown back, more water can be produced from the bottom, as illustrated by the more dramatic decrease in water saturation at a later stage. This observation is corroborated by the trend in gas production in **Figure 5-4**: the significant difference in the gas production between the base case and Case 1 at the early time can be attributed to water blocking; once the water in the bottom starts producing, the gas production rate for both cases would follow the same decline.

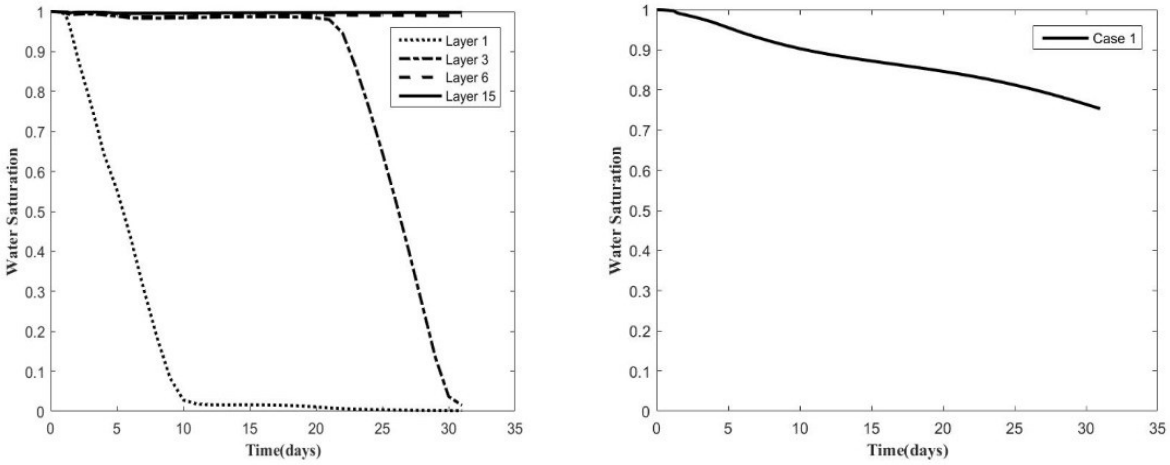

Figure 5-2 Comparison of water saturation profiles in the hydraulic fracture plane during the shut-in period between the base case and Case 1

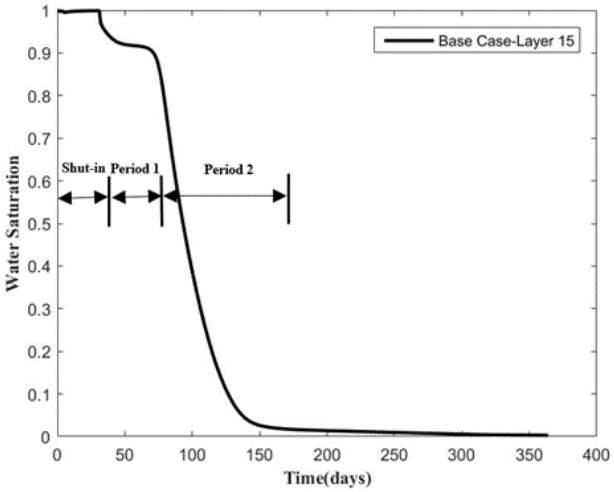

Figure 5-3 Water saturation profile in layer 15 (bottom of the hydraulic fracture plane) for the base case

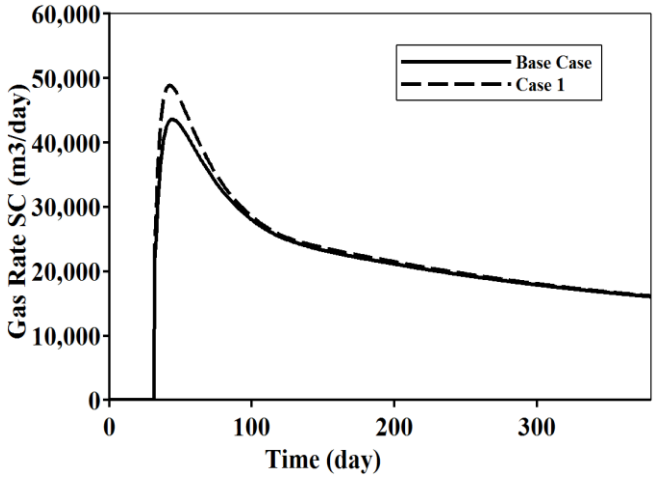

Figure 5-4 Comparison of gas production profiles between the base case and Case 1

It is expected that real fracture does not exist as a vertical plane. In fact, irregular packing and tortuosity in the fracture would impede gravity segregation. Case 2 is constructed by assuming $\tau = 10$ to model a tortuous fracture. Comparing the water saturation inside the hydraulic fracture plane at various depth as a function of time during the shut-in period in **Figure 5-5** confirms that gravity segregation is much less of an issue if tortuosity is considered. This is because the reduced fracture conductivity has effectively reduced water flux along the vertical direction. **Figure 5-6** compares the cumulative water production and average water saturation away from the fracture-matrix interface after 6 months of production between the base case and Case 2. It is interesting that Case 2 with a tortuous fracture has led to an approximate reduction of 20% in total water recovery. The results suggest the injected water is more likely to begin imbibing into the nearby matrix, instead of accumulating near the bottom of the reservoir. The driving force of capillarity is more significant when gravity effect is subdued.

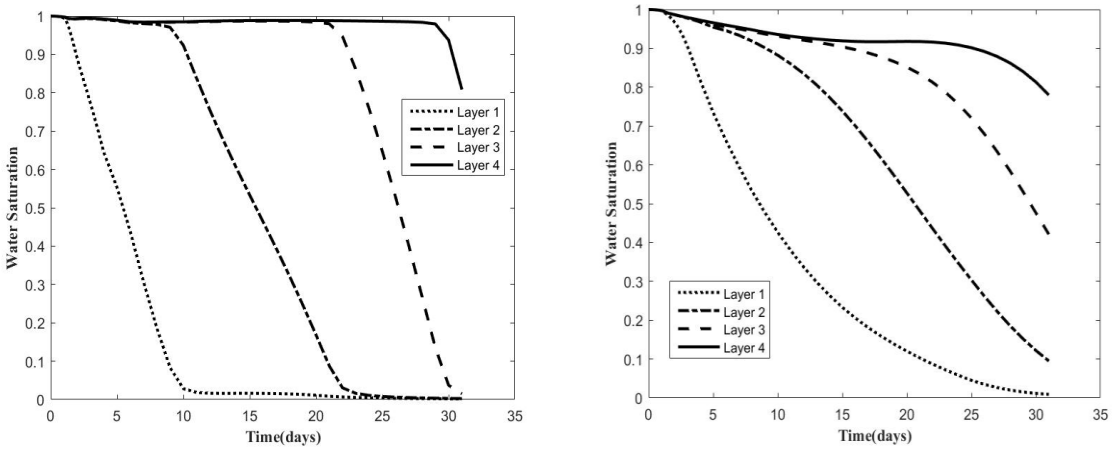

Figure 5-5 Comparison of water saturation profiles in the hydraulic fracture plane during the shut-in period between the base case (left) and Case 2 (right)

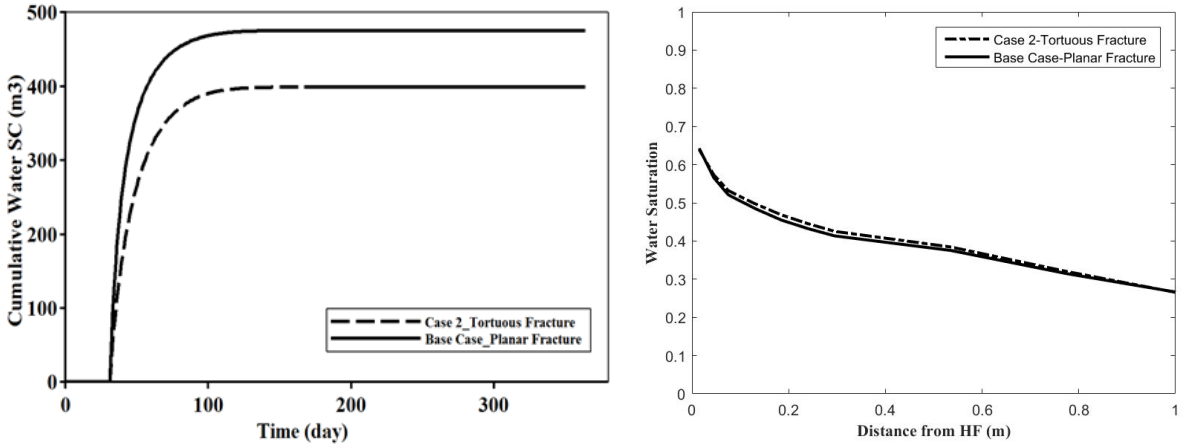

Figure 5-6 Comparison of cumulative water production or total water recovery (left) and the average water saturation as a function of distance away from the fracture-matrix interface (right)

5.4 Proppant Distribution and Post-Closure Fracture Geometry

In this section, non-uniform proppant distribution is modeled in cases 3 and 4, where only half of the fracture is filled with proppant. In case 3, the residual opening is not modeled, while in case 2, the residual opening is modeled explicitly. Fracture conductivity is considered to be proportional to proppant concentration under a wide range of closure stress, according to experimental data reported by Zhang et al. (2014). Therefore, it is assumed that the propped fracture conductivity at a given closure stress in these two cases is twice of that in the base case (Yu et al. 2015; Sierra et al. 2014). The well is shut in for 31 days (one month), which is followed by a production period of 334 days with a flowing bottom-hole pressure (P_{wf}) of 10 MPa.

The change in fracture conductivity with time during the shut-in and production periods for the Base Case and case 3 are compared in **Figure 5-7**, and the production profiles for all 3 cases are presented in **Figure 5-8**. A summary of the cases is presented in **Table 5-1**. As expected, the base case offers the highest cumulative gas production, because the hydraulic fracture is uniformly propped. Although the propped fracture conductivity in case 3 is two times that of the Base Case, the overall effectiveness of the fracture is reduced because the un-propped portion closes quickly upon stopping the injection. The cumulative water recovery is also lower for cases 3 and 4. The un-propped portion would experience a more significant reduction in fracture volume, driving more water to imbibe into the matrix (**Figure 5-9**).

Table 5-1 Summary of water and gas production of base case, case 3-7

	Peak rate (SC) (m^3/day)		**Cumulative production (SC) (m^3)**		**Remarks**	
	gas	**water**	**gas**	**water**	**BHP**	**Proppant Distribution**
Base Case	43535	46	7831700	504	P_{wf} = 10 MPa	Uniform
Case 3	38764	45	6882970	424	P_{wf} = 10 MPa	Non-Uniform Arch is not modeled
Case 4	47161	56	7336800	442	P_{wf} = 10 MPa	Non-Uniform Arch is modeled
Case 5	25129	28	4956970	393	P_{wf} = 20 MPa	Uniform
Case 6	23124	29	4777720	330	P_{wf} = 20 MPa	Non-Uniform Arch is not modeled
Case 7	27687	36	4605080	313	P_{wf} = 20 MPa	Non-Uniform Arch is modeled

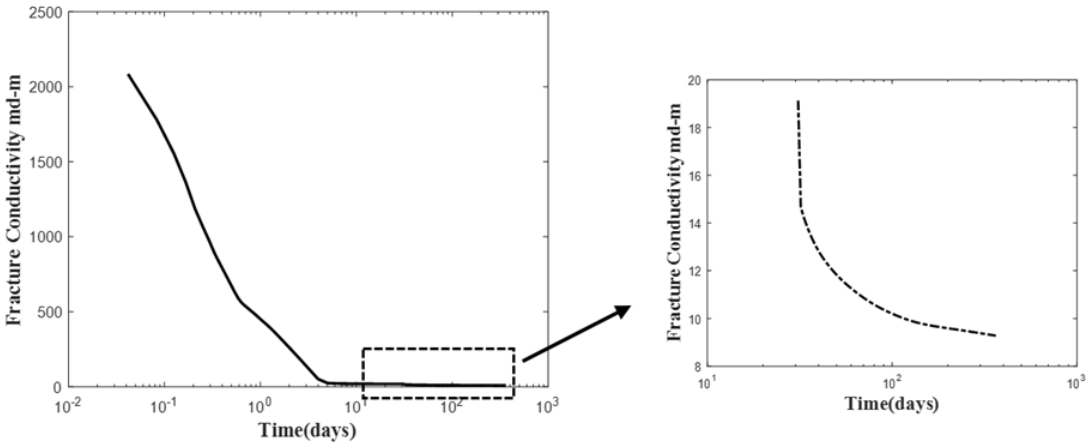

Base Case: uniform proppant distribution

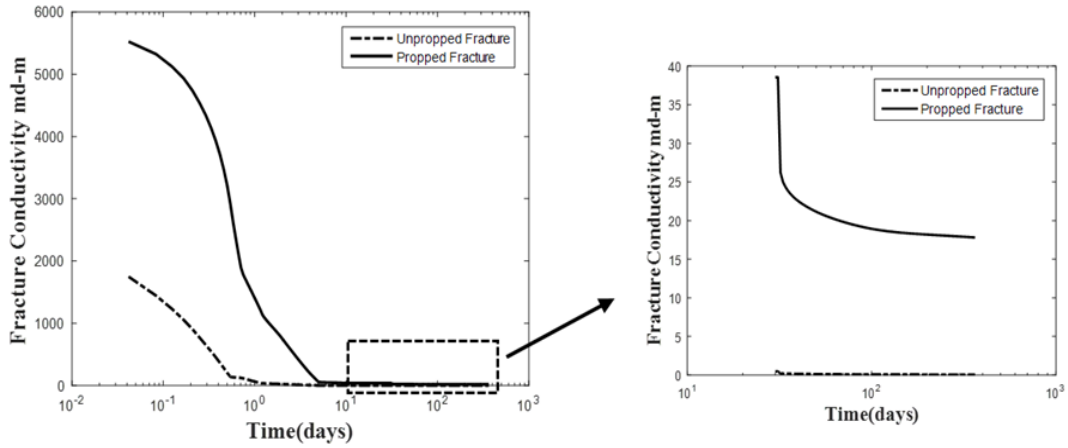

Case 3: non-uniform proppant distribution

Figure 5-7 Fracture conductivity profiles during shut-in and production

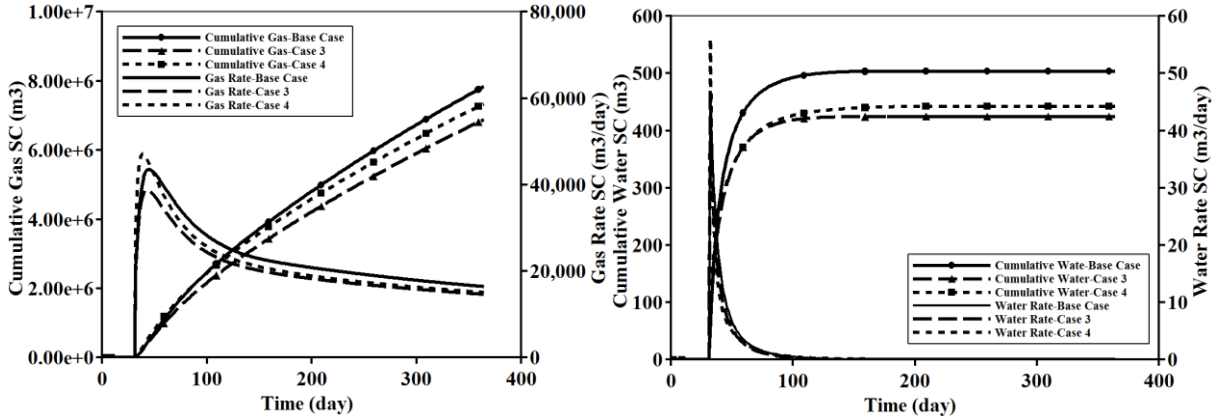

Figure 5-8 Production profiles of base case (uniform proppant distribution), case 3 (non-uniform proppant distribution; residual opening is not modeled) and case 4 (non-uniform proppant distribution; residual opening is modeled)

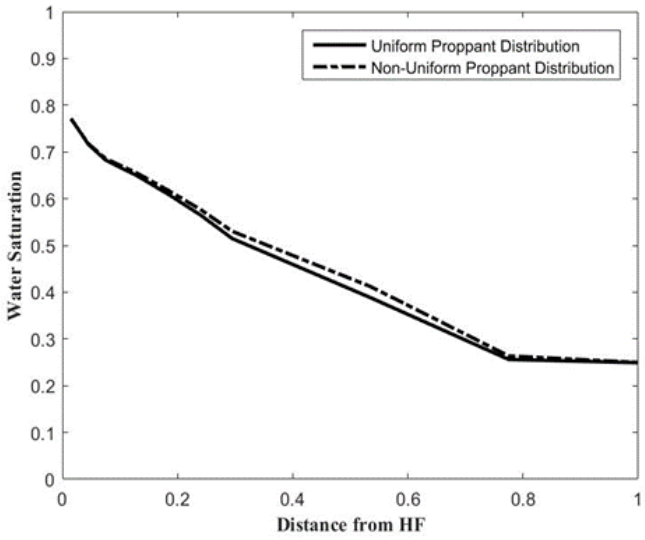

Figure 5-9 Comparison of matrix water saturation as a function of distance away from the fracture plane (m) at the end of shut-in between base case (solid line) and case 3 (dash line)

It is interesting to note that modeling the residual opening in case 4 would result in higher gas production when compared with case 3. The highly-conductive arch may enhance the initial gas

and water rates. However, any long-term enhancement is not obvious because of the closure of the propped portion. The combination of this highly-conductive residual opening and the un-propped fracture closure may contribute to the sharp production decline in shale gas wells. Comparing the water distribution across the fracture plane after 98 days of production (**Figure 5-10**), there is a significant amount of water pooling near the bottom in case 4, at least at the early production stage, while much of the water is recovered in case 3. High fluid velocities are expected in the residual opening because of its high conductivity. With a higher relative mobility, the gas phase competes favorably against the water phase; as a result, more water is retained and starts pooling near the bottom due to gravity. There are noticeable changes in the flow path near the residual opening. Comparing the phase velocities in **Figure 5-11**, it appears that the velocity distribution is more uniform in case 3. On the other hand, the high contrast in conductivity between the residual opening and the rest of the fracture plane causes significant distortion in the velocity distribution in case 4. Unfavorable gas-water displacement efficiency (Parmer et al. 2012), as evidenced by the high gas velocity along the vertical direction and reduced water velocity across the fracture plane for case 4, may contribute to the low water recovery during flowback. Nevertheless, the aggressive drawdown pressure (P_{wf} = 10 MPa) is sufficient to overcome gravity and capillarity effects, such that the final water recovery for case 4 is similar to case 3, although the time is takes to flow back all the recoverable water is much longer when the residual opening is modeled.

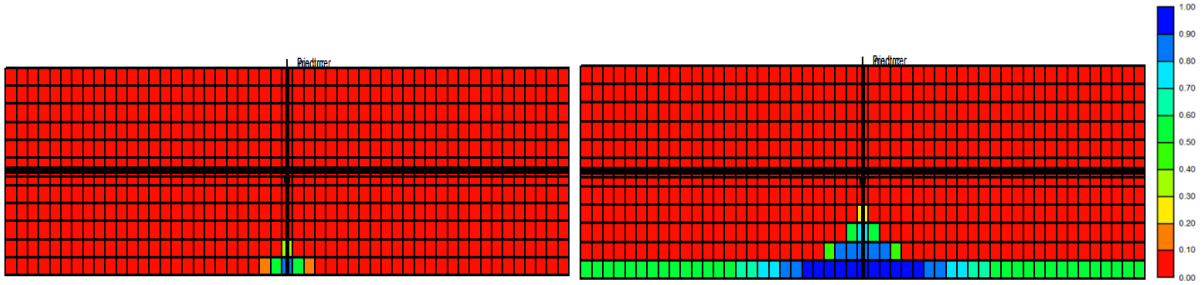

Figure 5-10 Water saturation distribution across the hydraulic fracture plane in Case 3 (left) and Case 4 (right) after 98 days of production

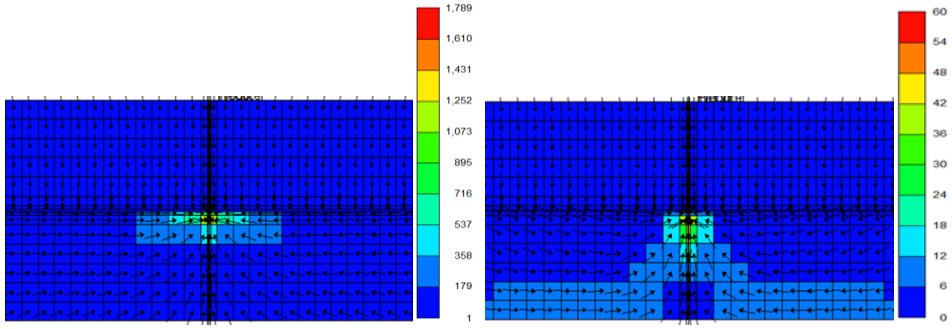

Case 3: residual opening is not modeled

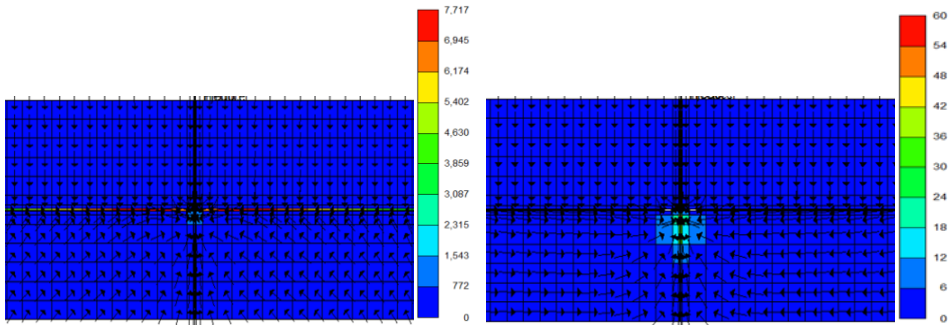

Case 4: residual opening is modeled

Figure 5-11 Velocity of gas (left) and water (right) phases in m/day across the fracture plane

5.5 Sensitivity to Drawdown Pressure and Shut-in Duration

The three cases are repeated using a less aggressive drawdown scheme (P_{wf}= 20 MPa) in cases 5-7. The production profiles are presented in **Figure 5-12**, and a summary is presented in **Table 5-1**. Trends similar to those in section 5.4 are observed. It is clear that less water is recovered for cases 5-7 with higher P_{wf}. Furthermore, comparing the water distribution across the fracture plane in **Figure 5-13** with **Figure 5-10**, it revealed that more water is retained in cases 5-7. **Figure 5-14** illustrates the matrix water saturation profiles at two different depths (h) for case 7. It is observed that even after producing for 100 days, the fracture water saturation at h =90 m has decreased from 1.0 to only 0.6, while the water saturation at h =110 m remains 1.0. Since imbibition is a slow process, water that is located near the top (closer to the perforation point) can be recovered during the early stage of production. When there is insufficient drawdown, water begins to accumulate near the bottom. As production continues, more water would imbibe into the nearby matrix. At h =110 m, it takes over 330 days for the water saturation in the hydraulic fracture to drop to 0.6. However, this water pooling is not permanent, as the water will slowly imbibe into the nearby matrix. The implication is that for a partially-propped fracture, aggressive drawdown is necessary to achieve high water flowback recovery. Insufficient drawdown would allow water to settle temporarily neat the bottom due to gravity and slowly imbibes into the nearby matrix.

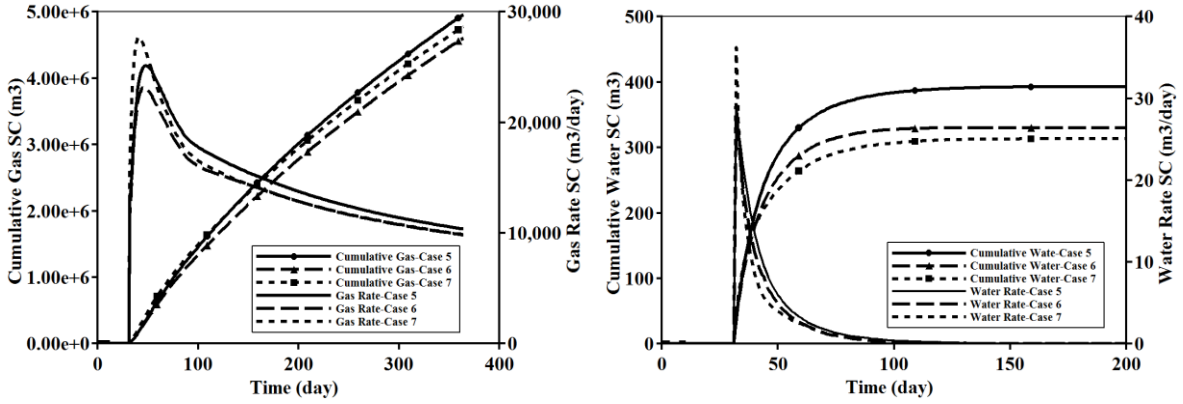

Figure 5-12 Production profiles of case 5 (uniform proppant distribution), case 6 (non-uniform proppant distribution; residual opening is not modeled) and case 7 (non-uniform proppant distribution; residual opening is modeled) with P_{wf} = 20 MPa

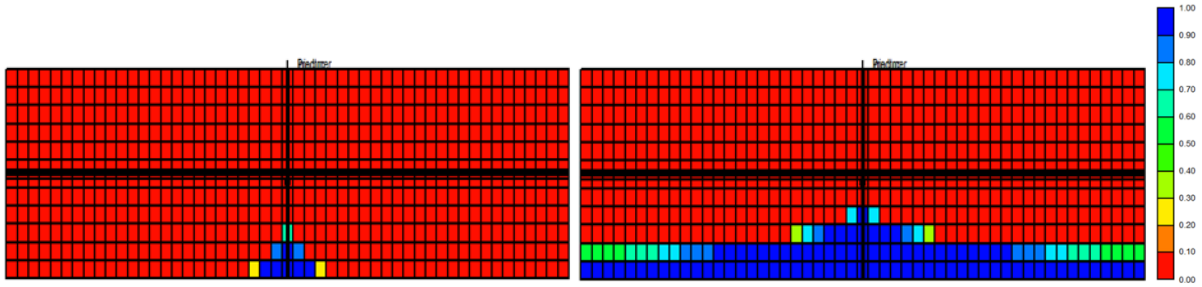

Figure 5-13 Water distribution across the hydraulic fracture plane in Case 6 (left, residual opening is not modeled) and Case 7 (right, residual opening is modeled) after 98 days of production

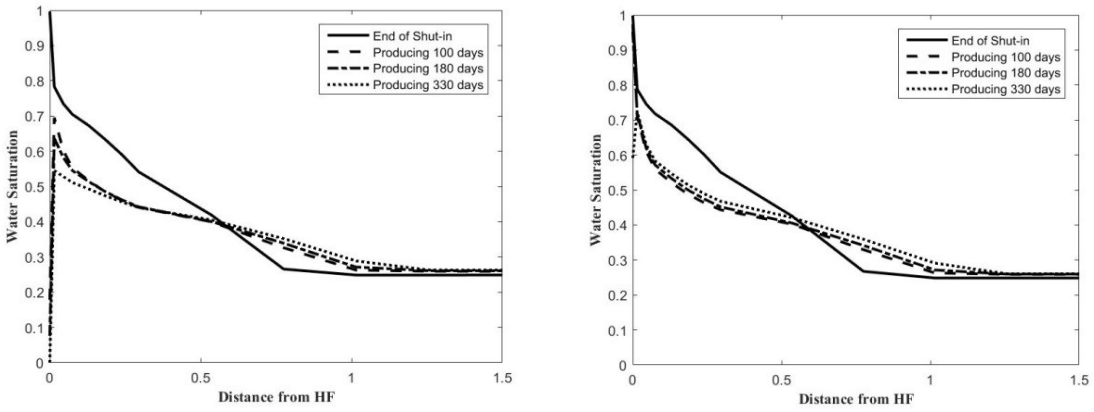

Figure 5-14 Water saturation as a function of distance (m) from fracture at two different depths (*h*) below the top of the reservoir for Case 7 (left: *h* = 90m; right: *h* = 110 m)

To encourage water imbibition into the matrix, extended shut-in is often proposed. Therefore, sensitivity analysis is performed to investigate whether prolonged shut-in may mitigate water retention when drawdown is low. Cases 8-10 are the same as case 7, except for the shut-in duration. Production characteristics of the three cases, as well as case 7, are summarized in **Table 5-2,** and the individual production profiles are presented in **Figure 5-15**. As expected, the peak gas rate increases, while the water recovery decreases, as the shut-in duration increases. However, long-term improvement in production is not observed: after producing for 365 days, prolonged shut-in results in a lower gas rate, and the cumulative gas production after one year is essentially the same for all cases. This observation is consistent with previous studies (Wang and Leung 2015; 2016). In the long-term, higher water saturation in the matrix could reduce gas flow by reducing its relative permeability. Considering imbibition is a slow and dynamic process, it is especially important to optimize shut-in duration and to mitigate the potential negative impacts due to uneven proppant distribution.

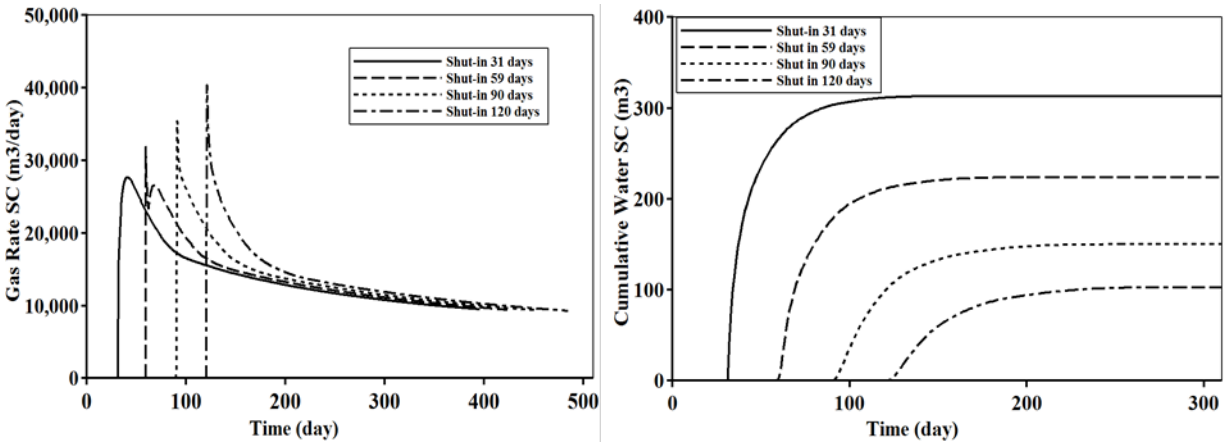

Figure 5-15 Gas rate and cumulative water recovery for cases with different shut-in duration (Cases 7-10)

Table 5-2 Summary of water and gas production of Cases 7-10

	Peak rate (SC) (m^3/day)		Cumulative water production (SC) (m^3)	Cumulative Gas production (SC) (10^6 m^3)	Gas rate after producing 365 days	Remarks	
	gas	water				BHP	Shut-in Time
Case 7	27687	36	313	5.08	9512	P_{wf} = 20 MPa	31 days
Case 8	31897	17	234	4.99	9428	P_{wf} = 20 MPa	59 days
Case 9	35426	4.7	150	4.89	9377	P_{wf} = 20 MPa	90 days
Case 10	40377	2.7	103	4.85	9278	P_{wf} = 20 MPa	120 days

5.6 Summary

The impacts of fracture closure, gravity segregation, fracture tortuosity, proppant distribution and post-closure geometry of a partially-propped fracture on fracturing fluid recovery and ensuring distribution have been discussed. Water uptake into the matrix is influenced by forced and spontaneous imbibition due to the large pressure differential across the matrix-fracture interface and matrix capillarity. Fracture closure forces more water to imbibe into the matrix. Gravity segregation may lead to water pooling near the bottom of a vertical planar fracture, but fracture tortuosity could limit the segregation and promote a more uniform fluid distribution. Matrix imbibition plays a more significant role in fracturing fluid distribution when gravity segregation is subdued. The residual opening after partially-propped fracture closure would exaggerate the effects of gravity segregation and hamper water recovery by providing a highly conductive flow path to gas flow. The implication is that more aggressive drawdown should be implemented to flow back the fracturing fluid. Extended shut-in duration would result in higher initial gas production and lower ultimate water recovery. However, long-term improvement in gas production is not observed.

Chapter 6 Field Case Study

6.1 Overview

Even proppant placement is generally not the case in actual field application; however, it is often assumed in most analytical and numerical models. In addition, complexity of fracture geometry is usually ignored in multi-cluster fractured wells. In this chapter, production data from two actual shale-gas wells is analyzed. The objectives are to determine whether accounting for various complexities discussed in the previous chapters (i.e., fracture closure, uneven proppant distribution) would impact the analysis of flowback production data and the potential implications on production forecast, as well as to assess the impact of complex fracture geometries due to stress-shadow effect on well performance in multi-cluster fracturing treatment.

6.2 Well Information

Two wells, b-G18-I/94-0-08 (well BG) and b-D18-I/94-0-08 (well BD), as shown in **Figure 6-1**, which were drilled in the Otter Park member of the Horn River Basin (Anderson et al. 2013) are used in this study. They are selected for this study because microseismic and gas production data analysis, previously conducted by Yousefzadeh et al. (2016), have concluded that less inter-well interference is observed in these wells, in comparison to other nearby wells. **Table 6-1** summarizes the completion and operation constraints of these two wells. The bottom-hole pressure was estimated from surface casing pressure measurements (Anderson et al. 2013). PVT data is extracted from Xu et al. (2016).

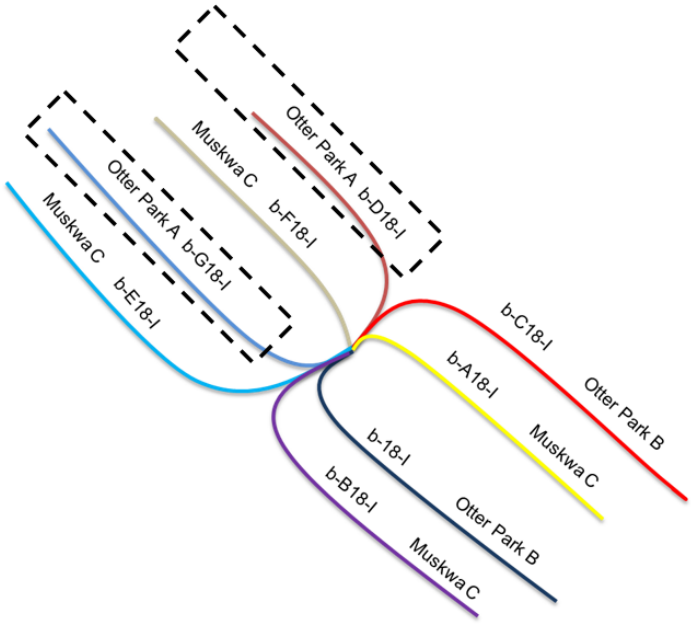

Figure 6-1 Schematic of the well pad contains well BG and well BD

Table 6-1 Completion and operation constraints of two Horn River wells in the Case Study

Well ID	Fracture stages	Perforation clusters	Fracture spacing (m)	Total injection volume (m^3)	Shut-in duration (days)
BG	20	1	100	75504	84
BD	15	4	25	60590	106

6.3 Case Study 1 – Well BG

This well consists of single cluster perforation for each fracture stage. A numerical model corresponding to a single fracture stage is constructed; the maximum fracture length is estimated from the total injection volume by assuming a planar fracture with an initial aperture of 0.03m. Three cases with different hydraulic fracture configuration are constructed (**Figure 6-2**). In Case A, the fracture is assumed to be evenly propped along the entire fracture of maximum length. In

Case B, only 160 m of the fracture is filled with proppant, and this is the effective fracture length obtained by using the *Compound Linear Typecurve Theory* model from rate transient analysis (RTA) of the flowback gas production data (HIS Harmony 2016). Case C was obtained by tuning the proppant distribution to match the field water and gas production data from the flowback period. In both Case B and Case C, the residual opening (arch) between the propped and un-propped segments is modeled according to section 3.2.

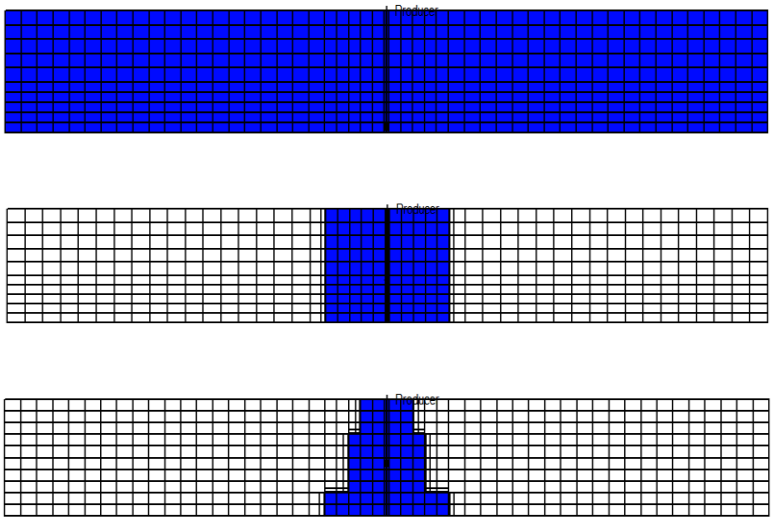

Figure 6-2 Proppant distribution along the fracture plane for Case A (top), Case B (middle) and Case C (bottom) – blue: with proppant; white: without proppant

Figure 6-3 shows the comparison between actual field data and the simulated production profiles for the three cases. It is clear that the production from Case A is too high, as it is assumed that all the injected fluid is injected to create an open fracture of maximum length. A more realistic assumption is that part of the hydraulic fracture is closed following the injection period. For both Case B and Case C, a reasonable match of gas production with field data is achieved. There is some deviation at the early stage of flowback, and it may be explained by the uncertainty in

estimating the bottom-hole pressure from surface casing pressure measurements due to complex wellbore effects such as liquid loading. However, when comparing the water production profiles, it is clear that the simulated profile for Case B is too low. This is because water production is not incorporated in most analytical models (like the one used in the RTA). On the other hand, a close match with the field data is obtained using the fracture configuration in Case C. It is obvious that, comparing the fracture configuration for Case B and Case C, the effective fracture length of Case C is slightly smaller. However, as discussed in section 5.4, a partially-propped fracture may lead to higher initial gas and water production. As a result, despite of its reduced effective fracture length, higher water production is obtained, while still achieving a reasonable match with the gas production data, in Case C. It should be noted that though the matrix properties are adjusted slightly from the ones used in Case B, a reasonable match with both the gas production data and water production data could not be attained without modifying the proppant distribution in the hydraulic fracture.

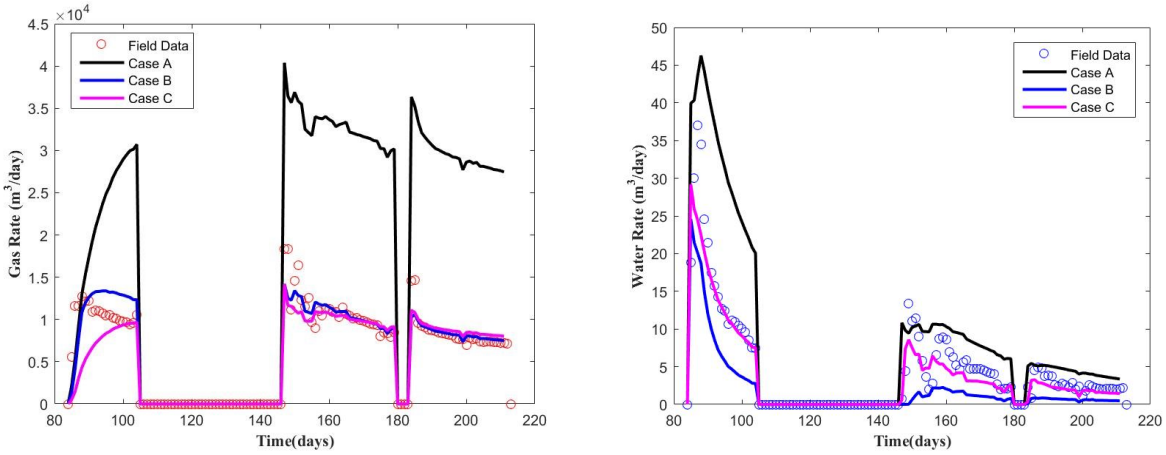

Figure 6-3 History-matching of flowback data for Cases A-C

To assess the forecast reliability of each model, the production forecast for both cases are compared in **Figure 6-4**. It is observed that the prediction using Case C resembles more closely to the field data over much of the forecast period. It is difficult to match some of the extremely high rates, which are likely the result of operational issues that have not been reflected in the daily-averaged surface casing pressure used in this study. In fact, an approximately 10% difference in the gas production is observed between the two cases. Given that production data analysis and history matching often provides solutions that are non-unique, additional realizations of the hydraulic configurations can be constructed to quantify the uncertainty. Nevertheless, the findings in this case study would suggest that incorporating additional physical mechanisms and heterogeneous fracture properties could improve model accuracy and forecast reliability.

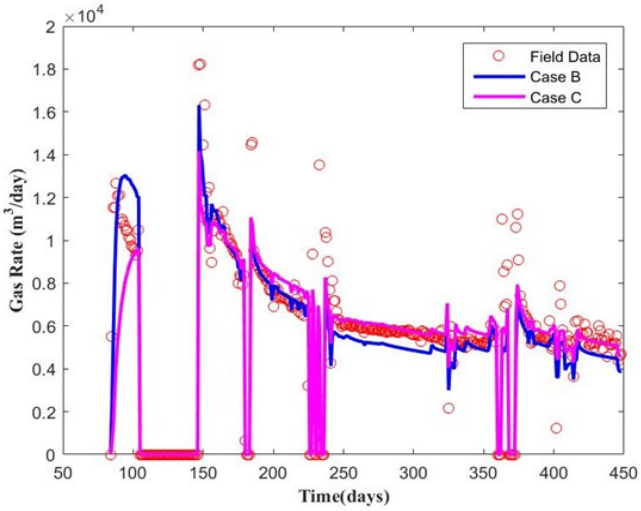

Figure 6-4 Gas production forecast for Case B and Case C

6.4 Case Study 2 – Well BD

The effect of stress shadow and proppant distribution in multi-cluster fracturing is examined in this section. In contrast to Well BG, each fracture stage in Well BD consists of 4 clusters of perforations. Previous field observations and modeling results indicated that non-uniform fractures would develop in multi-cluster fracturing (Wheaton et al. 2014; Wu et al. 2016). A numerical model corresponding to a single fracture stage is constructed, and two cases with different fracture geometries are constructed to match the production history. In Case D, 4 uniform fractures with an initial fracture aperture of 0.02 m are assumed. In Case E, non-uniform fracture geometry is assigned: to model the stress-shadow effect, the ratio of fracturing fluid distribution among fracture 1, 2, 3, and 4 is assumed to be 4:1:1:4, while the initial fracture aperture among fracture 1, 2, 3 and 4 is 0.025 m, 0.01 m, 0.01 m, and 0.025 m, respectively. Fracture configurations for these two cases, including proppant distribution, fracture half-length, and spacing are illustrated in **Figure 6-5**.

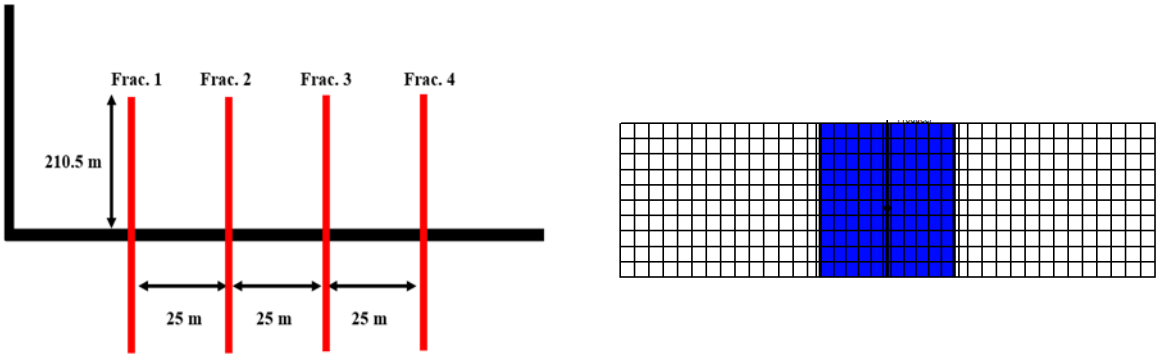

Case D: fracture geometry (left) and proppant distribution (right)

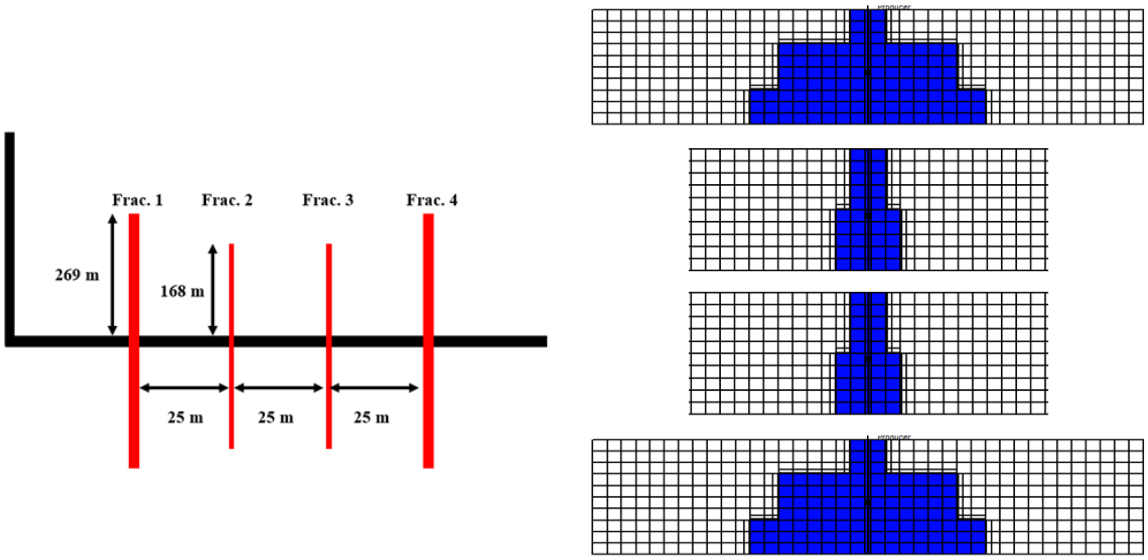

Case E: fracture geometries (left) and proppant distributions (right; top to bottom: Frac. 1 to Frac. 4)

Figure 6-5 Fracture geometry and proppant distribution along each fracture plane of a multi-cluster fracturing stage – blue: with proppant; white: without proppant (Well BD)

It is clear from the production profiles that both configurations can offer a close match to the actual history during the flow-back period (**Figure 6-6**) and the early production stage (**Figure 6-7**), despite some deviation in the late-time performance. Slightly lower production is observed in the case with uniform fractures (Case D) due to increased interference between the four closely-spaced fractures. This observation corroborates with the findings in Yu et al. (2014), who postulated that (1) outer fractures would contribute more to the total gas production when fracture spacing is small and (2) longer outer fractures would enhance gas production. It is interesting to note that ignoring the variability in fracture geometry due to stress-shadow effect could lead to a significant difference in the long-term cumulative gas production.

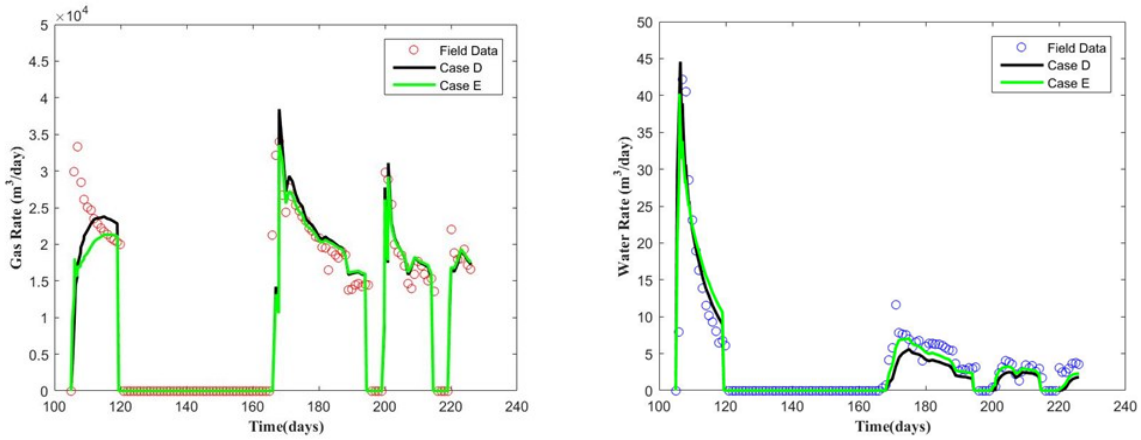

Figure 6-6 History matching of flowback data for Case D and Case E (Well BD)

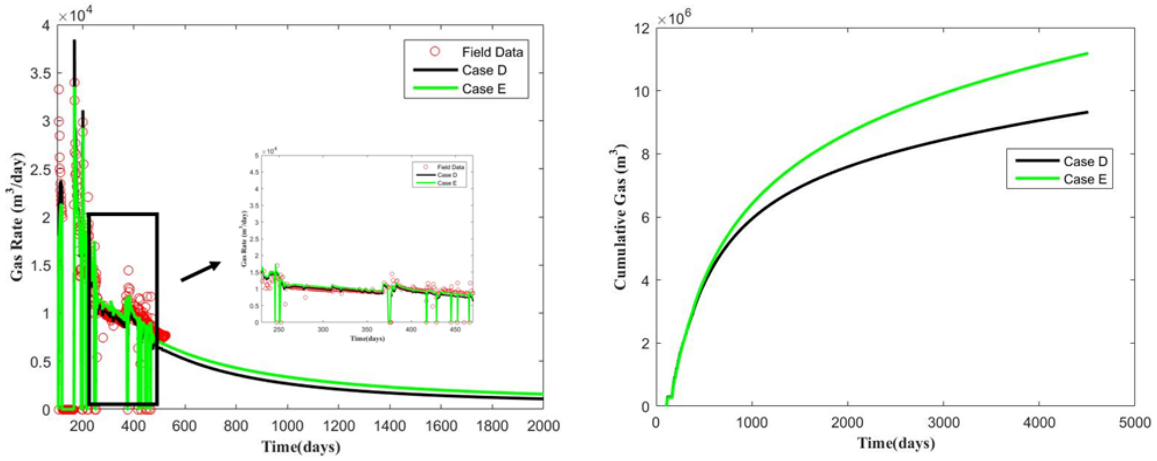

Figure 6-7 Gas production forecast for Case D and Case E (Well BD)

6.5 Summary

Result from the field case study demonstrates that accounting for variability in proppant distribution helps to improve history matching of gas and water production data during the flowback period, as well as the forecast reliability of the updated model. Fracture interference in

multi-cluster perforation treatments with small fracture spacing may hinder the long-term gas production. Longer outer fractures (due to stress-shadow effect) could contribute significantly to gas production. Understanding that the solution to an inverse problem is generally non-unique, the findings highlight the additional uncertainty in production forecast, when the effects of proppant distribution are ignored.

Chapter 7 Conclusion and Future Work

7.1 Overview

The closure behavior and post-closure geometry of a partially-propped fracture are investigated through geomechanical simulation. And the impacts of some potential contributing factors, such as fracture closure, proppant distribution, gravity segregation, on fracturing fluid recovery and in-situ distribution are examined by multi-phase flow simulations. The key conclusions and recommendations for future work are presented in this chapter.

7.2 Key Conclusions

1. Fracture closure behavior of a partially-propped fracture is investigated through geomechanical simulation. The geomechanical model is constructed under realistic rock properties and in-situ stress condition. Three distinct post-closure regions of a partially-propped fracture are identified: the lower propped zone (propped fracture), the upper closed un-propped zone (un-propped fracture) and the middle residual opening of un-propped zone (arch).

2. The size of the residual opening (arch) is most sensitive to the initial fracture aperture. The secondary fractures and anisotropic stress state have little impacts on the post-closure geometry of a partially-propped fracture, under the assumptions that the hydraulic fracture is orthogonal to the minimum in-situ stress and rock exhibits linear elasticity.

3. If proppant pack compaction is considered, it is observed that largest deformation is experienced near the top of the proppant pack due to stress amplification.

4. Modeling of fracture closure, gravity segregation and uneven proppant distribution (e.g., a tortuous partially-propped fracture) are coupled in the numerical simulation of fracturing fluid distribution and recovery. The focus is to examine the implications and uncertainties for ignoring these complexities when analyzing flowback and production data.

5. If fracture volume reduction during closure is ignored, the model overestimates the final water recovery by approximately 40% but underestimates the water recovery during the early stage of production or flowback in the case studies. This is because, during the shut-in period, decreasing fracture volume has driven more water to imbibe into matrix.

6. Gravity segregation is significant in vertical planar fracture. However, when fracture tortuosity is accounted for, the impacts of gravity segregation is dampened dramatically. Lower fracture conductivity due to tortuosity can reduce water flow along the vertical direction and subsequent water recovery (approximately 20% reduction in the case studies). Water imbibition into the nearby matrix due to capillarity becomes more prominent when gravity effect has been subdued.

7. For the same amount of injected fracturing fluid and proppant, uneven proppant distribution would contribute to a lower water recovery. The un-propped portion would experience a more significant reduction in fracture volume, driving more water to imbibe into the matrix.

8. Formation of a highly conductive residual opening after a partially-propped fracture closes has some complex implications on the ensuing gas and water flows. Gas tends to flow upward to the residual opening, the direction of which is against the gravity, resulting in un-

favorable gas-water displacement. The water flow rate is severely reduced due to this un-favorable gas-water displacement leading to more water retention in the hydraulic fracture.

9. Longer shut-in duration may enhance the initial gas rate, but no benefit is observed in the long-term production.

10. Result from the field case study demonstrates that heterogeneous fracture properties need to be considered when analyzing field data. Fracture interference in multi-cluster perforation treatments with small fracture spacing may hinder the long-term gas production. Longer outer fractures (due to stress-shadow effect) could contribute significantly to gas production. Understanding that the solution to an inverse problem is generally non-unique, the findings highlight the additional uncertainty in production forecast, when the effects of proppant distribution are ignored.

7.3 Future Work

1. The hydraulic fracture aperture and permeability usually vary along the fracture length, which could affect the fracturing fluid recovery and distribution. Incorporating more realistic hydraulic fracture explicitly into flow simulations could improve the model accuracy on analyzing the fluid flow and distribution. Thus, incorporating more realistic hydraulic fracture generated through a hydraulic-fracture-propagation model into flow models is recommended.

2. Since fracture propagates away from the perforation point progressively, it should be expected that more fracturing fluid leak-off occurs near the wellbore compared with that near the tip of the fracture (Zanganeh et al. 2015), which may result in uneven fluid distribution in the matrix away from the wellbore. Thus, in such reservoirs that leak-off during fracture propagation

stage is too significant to be ignored, the uneven matrix water saturation profile in vicinity of the fracture at the end of injection is recommended to be considered.

3. According to Sharma and Manchanda (2015), the induced un-propped fractures, which refers to fractures created around the main hydraulic fracture that are too small to accommodate any proppant, play a role in unconventional oil and gas wells. These induced fractures include natural fractures, micro-fractures induced along bedding planes or other planes of weakness. These induced fractures can be re-activated through tensile failure or shear failure, caused by in-situ stress variations, during the fluid injection stage. Therefore, the impacts of these induced fractures on recovery and in-situ distribution of fracturing fluid and subsequent gas production are recommended to be investigated.

4. According to Kim and Moridis (2014), compaction in the undrained condition (most likely in the extremely low-permeability shale gas reservoirs) could induce the increase of pore pressure, which can change effective-stress fields significantly and may result in rock shear failure (secondary fracturing). These secondary fractures increase the permeability significantly, and change the flow pattern, which, in turn, causes changes in the geomechanical variables. To capture these complicated physics in shale reservoirs, tightly coupled flow and geomechanical models are highly recommended to describe the reservoir behaviors accurately in the long term.

5. In clay-rich reservoirs, the interaction between fracturing fluid and rock can cause permanent damage for absolute matrix permeability, due to clay swelling. The effect of clay swelling is recommended to be incorporated into the analysis of fracturing fluid flowback and subsequent gas production.

Bibliography

Abbasi, M., Dehghanpour, H. and Hawkes, R.V. 2012. Flowback analysis for fracture characterization. Presented at the SPE Canadian Unconventional Resources Conference, Calgary, Alberta, Canada, 30 October-1 November. SPE-162661-MS.

Abbasi, M.A., Ezulike, D.O., Dehghanpour, H. et al. 2014. A comparative study of flowback rate and pressure transient behavior in multifractured horizontal wells completed in tight gas and oil reservoirs. *Journal of Natural Gas Science and Engineering*, **17**: 82-93.

Acharya, A.R. 1986. Particle transport in viscous and viscoelastic fracturing fluids. *SPE Production Engineering*, **1** (02): 104-110. SPE-13179-PA.

Agrawal, S. and Sharma, M.M. 2015. Practical insights into liquid loading within hydraulic fractures and potential unconventional gas reservoir optimization strategies. *Journal of Unconventional Oil and Gas Resources*, **11:** 60-74.

Alkouh, A., McKetta, S. and Wattenbarger, R.A. 2014. Estimation of effective-fracture volume using water-flowback and production data for shale-gas wells. *Journal of Canadian Petroleum Technology*, **53** (05): 290-303. SPE-166279-PA.

Alotaibi, M.A. and Miskimins, J.L. 2015. Slickwater Proppant Transport in Complex Fractures: New Experimental Findings & Scalable Correlation. Presented at the SPE Annual Technical Conference and Exhibition, Houston, Texas, USA, 28-30 September. SPE-174828-MS.

Alramahi, B. and Sundberg, M.I. 2012. Proppant embedment and conductivity of hydraulic fractures in shales. Presented at the 46th US Rock Mechanics/Geomechanics Symposium, Chicago, Illinois, USA, 24-27 June. ARMA-2012-291.

Amadei, B. and Goodman, R.E. 1981. Formulation of complete plane strain problems for regularly jointed rocks. Presented at the 22nd US Symposium on Rock Mechanics, Cambridge, Massachusetts, 29 June-2 July. ARMA-81-0245

Anderson, D.M., Turco, F., Virues, C.J.J. et al. 2013. Application of Rate Transient Analysis Workflow in Unconventional Reservoirs: Horn River Shale Gas Case Study. Presented at the SPE Unconventional Resources Conference and Exhibition-Asia Pacific, Brisbane, Australia, 11-13 November. SPE-167042-MS.

Bertoncello, A., Wallace, J., Blyton, C. et al. 2014. Imbibition and water blockage in unconventional reservoirs: well management implications during flowback and early production. *SPE Reservoir Evaluation & Engineering*, **17**(04): 497-506. SPE-167698-PA.

Bradley, H. B. ed. 1992. *Petroleum Engineering Handbook*, third edition, Chap. 26. Richardson, Texas: SPE.

Chalmers, G.R., Ross, D.J. and Bustin, R.M. 2012. Geological controls on matrix permeability of Devonian Gas Shales in the Horn River and Liard basins, northeastern British Columbia, Canada. *International Journal of Coal Geology*, **103**: 120-131.

Chen, D., Pan, Z. and Ye, Z. 2015. Dependence of gas shale fracture permeability on effective stress and reservoir pressure: model match and insights. Fuel, 139: 383-392.

Cheng, Y. 2012. Impact of Water Dynamics in Fractures on the Performance of Hydraulically Fractured Wells in Gas-Shale Reservoirs. *Journal of Canadian Petroleum Technology* **51** (2): 143-151. SPE-127863-PA.

Cho, Y., Ozkan, E. and Apaydin, O.G. 2013. Pressure-dependent natural-fracture permeability in shale and its effect on shale-gas well production. *SPE Reservoir Evaluation & Engineering*, **16** (02): 216-228. SPE-159801-PA.

Chou, Q., Gao, H.J. and Somerwil, M. 2011. Analysis of Geomechanical Data for Horn River Basin Gas Shales, North-East British Columbia, Canada. Presented at the SPE Middle East Unconventional Gas Conference and Exhibition, Muscat, Oman, 31 January-2 February. SPE-142498-MS.

Cipolla, C.L., Lolon, E., Mayerhofer, M.J. and Warpinski, N.R. 2009. The effect of proppant distribution and un-propped fracture conductivity on well performance in unconventional gas reservoirs. Presented at the SPE Hydraulic Fracturing Technology Conference, The Woodlands, Texas, USA, 19-21 January. SPE-119368-MS.

Clark, P.E. and Quadir, J.A. 1981. Prop transport in hydraulic fractures: a critical review of particle settling velocity equations. Presented at the SPE/DOE Low Permeability Gas Reservoirs Symposium, Denver, Colorado, USA, 27-29 May. SPE-9866-MS.

Computer Modeling Group. 2015. *GEM: Compositional & Unconventional Reservoir Simulator User's Guide (Version 2015)*. Computer Modeling Group Limited, Calgary.

Crafton, J.W. 2010. Flowback performance in intensely naturally fractured shale gas reservoirs. Presented at the SPE Unconventional Gas Conference, Pittsburgh, Pennsylvania, USA, 23-25 February. SPE-131785-MS.

Crafton, J.W. and Noe, S. 2013. Factors Affecting Early Well Productivity in Six Shale Plays. Presented at the SPE Annual Technical Conference and Exhibition, Orleans, Louisiana, USA, 30 September-2 October. SPE-166101-MS.

Daneshy, A.A. 2005. Proppant Distribution and Flowback in Off-Balance Hydraulic Fractures. SPE Production & Facilities, **20** (01): 41-47. SPE-89889-PA.

Dayan, A., Stracener, S.M. and Clark, P.E. 2009. Proppant transport in slickwater fracturing of shale gas formations. Presented at the SPE Annual Technical Conference and Exhibition, New Orleans, Louisiana, USA, 4-7 October. SPE-125068-MS.

Deshpande, Y.K., Crespo, F., Bokane, A.B. et al. 2013. Computational fluid dynamics (CFD) study and investigation of proppant transport and distribution in multistage fractured horizontal wells. Presented at the SPE Reservoir Characterization and Simulation Conference and Exhibition, Abu Dhabi, UAE, 16-18 September. SPE-165952-MS.

Economides, M. J. and Nolte, K. G. 2000. *Reservoir Stimulation*. Wiley.

Ehlig-Economides, C.A., Ahmed, I.A., Apiwathanasorn, S. et al. 2012. Stimulated Shale Volume Characterization: Multiwell Case Study from the Horn River Shale: II. Flow Perspective. Presented at the SPE Annual Technical Conference and Exhibition, San Antonio, Texas, USA, 8-10 October. SPE-159546-MS.

Ezulike, O., Dehghanpour, H., Virues, C. et al. 2016. Flowback Fracture Closure: A Key Factor for Estimating Effective Pore Volume. *SPE Reservoir Evaluation & Engineering,* **19** (04): 567-582. SPE-175143-PA.

Evans, R.D. and Civan, F. 1994. Characterization of non-Darcy multiphase flow in petroleum bearing formation. Final report (No. DOE/BC/14659--7), School of Petroleum and Geological Engineering, Oklahoma University, Oklahoma.

Fakcharoenphol, P., Torcuk, M.A., Wallace, J. et al. 2013. Managing shut-in time to enhance gas flow rate in hydraulic fractured shale reservoirs: a simulation study. Presented at the SPE Annual Technical Conference and Exhibition, New Orleans, Louisiana, USA, 30 September-2 October. SPE-166098-MS.

Fan, L., Thompson, J.W. and Robinson, J.R. 2010. Understanding gas production mechanism and effectiveness of well stimulation in the Haynesville Shale through reservoir simulation. Presented at the Canadian Unconventional Resources and International Petroleum Conference, Calgary, Alberta, Canadam 19-21 October. SPE-136696-MS.

Fisher, M.K. and Warpinski, N.R. 2012. Hydraulic-fracture-height growth: Real data. *SPE Production & Operations*, **27**(01): 8-19. SPE-145949-PA.

Fredd, C.N., McConnell, S.B., Boney, C.L. et al. 2001. Experimental study of fracture conductivity for water-fracturing and conventional fracturing applications. *SPE Journal*, **6** (03): 288-298. SPE-74138-PA.

Gensterblum, Y., Ghanizadeh, A., Cuss, R.J et al. 2015. Gas transport and storage capacity in shale gas reservoirs–A review. Part A: transport processes. *Journal of Unconventional Oil and Gas Resources*, **12:** 87-122.

Gdanski, R.D. and Walters, H.G. 2010. Impact of fracture conductivity and matrix relative permeability on load recovery. Presented at the SPE Annual Technical Conference and Exhibition, Florence, Italy, 19-22 September. SPE-133057-MS.

Gdanski, R.D., Fulton, D.D. and Shen, C. 2009. Fracture-Face-Skin Evolution During Cleanup. *SPE Production & Operations*, **24** (01): 22-34. SPE-101083-PA.

Ghanbari, E. and Dehghanpour, H. 2016. The fate of fracturing water: A field and simulation study. *Fuel*, **163:** 282-294.

Gu, F. and Chalaturnyk, R. 2010. Permeability and porosity models considering anisotropy and discontinuity of coalbeds and application in coupled simulation. *Journal of Petroleum Science and Engineering*, **74**(3): 113-131.

Holditch, S.A. 1979. Factors affecting water blocking and gas flow from hydraulically fractured gas wells. *Journal of Petroleum Technology*, **31**(12): 1-515. SPE-7561-PA.

Holditch, A.S. and Tschirhart, N. 2005. Optimal Stimulation Treatments in Tight Gas Sands. Presented at the SPE Annual Technical Conference and Exhibition, Dallas, Texas, 9-12 October. SPE-96104-MS.

Huang, J. and Ghassemi, A. 2012. Geomechanical evolution of fractured reservoirs during gas production. Presented at the 46th US Rock Mechanics/Geomechanics Symposium, Chicago, Illinois, USA, 24-27 June. ARMA-2012-321.

Huo, D., Li, B. and Benson, S.M. 2014. Investigating Aperture-Based Stress-Dependent Permeability and Capillary Pressure in Rock Fractures. Presented at the SPE Annual Technical Conference and Exhibition, Amsterdam, The Netherlands, 27-29 October. SPE-170819-MS.

IHS Harmony. 2016. Analysis Method Theory, IHS Inc. https://www.ihs.com/btp/fekete.html

Itasca. 2015. *FLAC: Two-dimensional Explicit Finite Difference Program User's Guide (Version 7.0)*. Itasca Limited.

Jansen, T.A., Zhu, D. and Hill, A.D. 2015. The effect of rock mechanical properties on fracture conductivity for shale formations. Presented at the SPE Hydraulic Fracturing Technology Conference, The Woodlands, Texas, USA, 3-5 Februray. SPE-173347-MS.

Kam, P., Nadeem, M., Novlesky, A. et al. 2015. Reservoir Characterization and History Matching of the Horn River Shale: An Integrated Geoscience and Reservoir-Simulation Approach. *Journal of Canadian Petroleum Technology*, **54** (6): 475-488. SPE-171611-PA.

Kern, L.R., Perkins, T.K. and Wyant, R.E. 1959. The mechanics of sand movement in fracturing. Journal of Petroleum Technology, 11 (07): 55-57. SPE-1108-G.

Khanna, A., Neto, L.B. and Kotousov, A. 2014. Effect of residual opening on the inflow performance of a hydraulic fracture. *International Journal of Engineering Science*, **74:** 80-90.

Kim, J. and Moridis, G.J. 2014. Gas flow tightly coupled to elastoplastic geomechanics for tight- and shale-gas reservoirs: Material failure and enhanced permeability. *SPE Journal*, **19**(06): 1-10.

King, G. E. 2012. Hydraulic Fracturing 101: What Every Representative, Environmentalist, Regulator, Reporter, Investor, University Researcher, Neighbor, and Engineer Should Know About Hydraulic Fracturing Risk, *Journal of Petroleum Technology*. **64** (04): 34-42.

Langmuir, I. 1918. The Adsorption of Gases on Plane Surfaces of Glass, Mica and Platinum. *Journal of the American Chemical society*, **40** (9): 1361-140.

Leverett, M. 1941. Capillary Behavior in Porous Solids. *Transactions of the AIME*, **142** (01): 152-169. SPE-941152-G.

Makhanov, K., Habibi, A., Dehghanpour, H. et al. 2014. Liquid Uptake of Gas Shales: A Workflow to Estimate Water Loss During Shut-in Periods After Fracturing Operations. Journal of Unconventional Oil and Gas Resources **7:** 22-32.

Mayerhofer, M.J. and Meehan, D.N. 1998. Waterfracs-results from 50 cotton valley wells. Presented at the SPE Annual Technical Conference and Exhibition, New Orleans, Louisiana, USA, 27-30 September. SPE-49104-MS.

McClure, M. 2014. The Potential Effect of Network Complexity on Recovery of Injected Fluid Following Hydraulic Fracturing. Presented at the SPE Unconventional Resources Conference, The Woodlands, Texas, USA, 1-3 April. SPE-168991-MS.

Nejadi, S., Leung, J.Y., Trivedi, J.J. et al. 2015. Integrated Characterization of Hydraulically Fractured Shale-Gas Reservoirs—Production History Matching. *SPE Reservoir Evaluation & Engineering,* **18** (4): 481-494. SPE-171664-PA.

Neto, L.B. and Kotousov, A. 2013. Residual opening of hydraulic fractures filled with compressible proppant. *International Journal of Rock Mechanics and Mining Sciences*, **61:** 223-230.

Novlesky, A., Kumar, A. and Merkle, S. 2011. Shale Gas Modeling Workflow: From Microseismic to Simulation--A Horn River Case Study. Presented at the Canadian Unconventional Resources Conference, Calgary, Alberta, Canada, 15-17 November. SPE-148710-MS.

Pagels, M., Hinkel, J.J. and Willberg, D.M. 2012. Measuring capillary pressure tells more than pretty pictures. Presented at the SPE International Symposium and Exhibition on Formation Damage Control, Lafayette, Louisiana, USA, 15-17 February. SPE-151729-MS.

Palisch, T.T., Duenckel, R.J., Bazan, L.W. et al. 2007. Determining realistic fracture conductivity and understanding its impact on well performance-theory and field examples. Presented at the SPE Hydraulic Fracturing Technology Conference, College Station, Texas, USA, 29-31 January. SPE-106301-MS.

Palisch, T.T., Vincent, M. and Handren, P.J. 2010. Slickwater fracturing: food for thought. *SPE Production & Operations*, **25** (03): 327-344. SPE-115766-PA.

Parmar, J., Dehghanpour, H. and Kuru, E. 2012. Unstable Displacement: a Missing Factor in Fracturing Fluid Recovery. Presented at the SPE Canadian Unconventional Resources Conference, Calgary, Alberta, Canada, 30 October-1 November. SPE-162649-MS.

Parmar, J., Kuru, E., and Dehghanpour, H. 2013. Drainage Against Gravity: Factors Impacting the Load Recovery in Fractures. Presented at the SPE Unconventional Resources Conference, The Woodlands, Texas, USA, 10-12 April. SPE-164530-MS.

Patankar, N.A., Joseph, D.D., Wang, J et al. 2002. Power law correlations for sediment transport in pressure driven channel flows. *International Journal of Multiphase Flow*, **28** (8): 1269-1292.

Sahai, R., Miskimins, J.L. and Olson, K.E. 2014. Laboratory results of proppant transport in complex fracture systems. Presented at the SPE Hydraulic Fracturing Technology Conference, the Woodlands, Texas, USA, 4-6 February. SPE-168579.

Shah, S.N., Mahmoud, A. and Lord, D.L. 2001. Proppant Transport Characterization of Hydraulic-Fracturing Fluids Using a High-Pressure Simulator Integrated With a Fiber-Optic/Light-Emitting-Diode (LED) Vision System. *SPE Production & Facilities*, **16** (01): 42-49. SPE-69210-PA.

Sharma, M.M. and Manchanda, R. 2015. The Role of Induced Un-propped (IU) Fractures in Unconventional Oil and Gas Wells. Presented at the SPE Annual Technical Conference and Exhibition, Houston, Texas, USA, 28-30 September. SPE-174946-MS.

Sherman, J.B. and Holditch, S.A. 1991. Effect of injected fracture fluids and operating procedures on ultimate gas recovery. Presented at the SPE Gas Technology Symposium, Houston, Texas, USA, 22-24 January. SPE-21496-MS.

Shiozawa, S. and McClure, M. 2016a. Simulation of proppant transport with gravitational settling and fracture closure in a three-dimensional hydraulic fracturing simulator. *Journal of Petroleum Science and Engineering*, **138:** 298-314.

Shiozawa, S. and McClure, M. 2016b. Comparison of Pseudo-3D and Fully-3D Simulations of Proppant Transport in Hydraulic Fractures, Including Gravitational Settling, Formation of Proppant Banks, Tip-Screen Out, and Fracture Closure. Presented at the SPE Hydraulic Fracturing Technology Conference, The Woodlands, Texas, USA, 9-11 February. SPE-179132-MS.

Sierra, L., Sahai, R.R. and Mayerhofer, M.J. 2014. Quantification of Proppant Distribution Effect on Well Productivity and Recovery Factor of Hydraulically Fractured Unconventional Reservoirs. Presented at the SPE/CSUR Unconventional Resources Conference, Calgary, Alberta, Canada, 30 September-2 October. SPE-171594-MS.

Tong, S. and Mohanty, K.K. 2016. Proppant transport study in fractures with intersections. *Fuel*, **181:** 463-477.

Wang, C., Wu, Y.S., Xiong, Y. et al. 2015. Geomechanics coupling simulation of fracture closure and its influence on gas production in shale gas reservoirs. Presented at the SPE Reservoir Simulation Symposium, Houston, Texas, USA, 23-25 February. SPE-173222-MS.

Wang, J.Y., Holditch, S. and McVay, D. 2010. Modeling Fracture-Fluid Cleanup in Tight-Gas Wells. *SPE Journal*, **15** (03): 783-793. SPE 119624-PA.

Wang, M. and Leung, J.Y. 2015. Numerical investigation of fluid-loss mechanisms during hydraulic fracturing flow-back operations in tight reservoirs. *Journal of Petroleum Science and Engineering*, **133:** 85-102.

Wang, M. and Leung, J.Y. 2016. Numerical investigation of coupling multiphase flow and geomechanical effects on water loss during hydraulic-fracturing flowback operation. *SPE Reservoir Evaluation & Engineering*, **19** (03): 520-537. SPE-178618-PA.

Wang, Y. and Aryana, S. 2016. Numerical investigation of stress-dependent fracture apertures and their spatial variations on production from unconventional gas reservoirs with complex fracture geometries. Presented at the SPE Low Perm Symposium, Denver, Colorado, USA, 5-6 May. SPE-180244-MS.

Warpinski, N.R. 2010. Stress Amplification and Arch Dimensions in Proppant Beds Deposited by Waterfracs. *SPE Production & Operations*, **25** (04): 461-471. SPE-119350-PA**.**

Wheaton, B., Miskimins, J., Wood, D. et al. 2014. Integration of distributed temperature and distributed acoustic survey results with hydraulic fracture modeling: a case study in the Woodford shale. Presented at the SPE/AAPG/SEG Unconventional Resources Technology Conference, Denver, Colorado, USA, 25-27 August. URTEC-1922140-MS.

Wu, K., Olson, J., Balhoff, M.T. et al. 2016. Numerical Analysis for Promoting Uniform Development of Simultaneous Multiple-Fracture Propagation in Horizontal Wells. *SPE Production & Operations*. SPE-174869-PA.

Wu, K. and Olson, J.E. 2016. Mechanisms of Simultaneous Hydraulic-Fracture Propagation From Multiple Perforation Clusters in Horizontal Wells. *SPE Journal*, **21** (3): 1,000-1,008. SPE-178925-PA.

Wu, Y.S., Li, J., Ding, D. et al. 2014. A generalized framework model for the simulation of gas production in unconventional gas reservoirs. *SPE Journal*, **19** (05): 845-857. SPE-163609-PA.

Xu, Y., Adefidipe, O. and Dehghanpour, H. 2016. A flowing material balance equation for two-phase flowback analysis. *Journal of Petroleum Science and Engineering*, **142:** 170-185.

Yousefzadeh, A., Li, Q., Virues, C. and Aguilera, R. 2016. Integrated Interpretation of Microseismic and Petroleum Engineering Data for Comparison of Gas Production in Two Interfering Adjacent Wellpads in the Horn River Basin, Canada. Presented at the Unconventional Resources Technology Conference, SanAntonio, Texas, USA, 1-3 August. URTEC-2460254-MS.

Yu, W. and Sepehrnoori, K. 2014. An efficient reservoir-simulation approach to design and optimize unconventional gas production. Journal of Canadian Petroleum Technology, 53 (02): 109-121. SPE-165343-PA.

Yu, W. Luo, Z. Javadpour, F. et al. 2014. Sensitivity analysis of hydraulic fracture geometry in shale gas reservoirs. *Journal of Petroleum Science and Engineering*, **113**: 1-7.

Yu, W., Zhang, T., Du, S. et al. 2015. Numerical study of the effect of uneven proppant distribution between multiple fractures on shale gas well performance. *Fuel*, **142**: 189-198.

Yue, M., Leung, J.Y. and Dehghanpour, H. 2016. Numerical Investigation of Limitations and Assumptions of Analytical Transient Flow Models in Tight Oil Reservoirs. *Journal of Natural Gas Science and Engineering*, **30**: 471-486.

Zanganeh, B., Ahmadi, M., Hanks, C. et al. 2015. The role of hydraulic fracture geometry and conductivity profile, unpropped zone conductivity and fracturing fluid flowback on production performance of shale oil wells. *Journal of Unconventional Oil and Gas Resources*, **9:** 103-113.

Zanganeh, B., Soroush, M., Williams-Kovacs, J.D. and Clarkson, C.R., 2015. Parameters Affecting Load Recovery and Oil Breakthrough Time after Hydraulic Fracturing in Tight Oil Wells. Presented at the SPE/CSUR Unconventional Resources Conference, Calgary, Alberta, Canada, 20-22 October. SPE-175941-MS.

Zhang, J. and Dunn-Norman, S. 2015. Computational Fluid Dynamics Modeling of Proppant Transport in a Plug and Perf Completion with Different Perforation Phasing. Presented at the Unconventional Resources Technology Conference, San Antonio, Texas, USA, 20-22 July. SPE-178654-MS.

Zhang, J., Kamenov, A., Hill, A.D. and Zhu, D. 2014. Laboratory Measurement of Hydraulic-Fracture Conductivities in the Barnett Shale. *SPE Production & Operations*, **29** (03): 216-227. SPE-163839-PA.

Zhou, Z. 2016. *The impact of capillary imbibition and osmosis during hydraulic fracturing of shale formations*. Doctoral dissertation, Colorado School of Mines. Arthur Lakes Library.

Zou, C. 2012. *Unconventional Petroleum Geology*, first edition, Newnes.